Chemical Science

ROYAL SOCIETY OF CHEMISTRY

PERSPECTIVE

View Article Online
View Journal | View Issue

Cite this: *Chem. Sci.*, 2026, **17**, 8835

All publication charges for this article have been paid for by the Royal Society of Chemistry

An experimental perspective on symmetry breaking and the singlet fission mechanism in solid-state materials

Xinyue Xu, Christopher R. Hall and Trevor A. Smith *

Singlet fission (SF) materials have attracted attention in the field of solar cell research for decades. The deployment of novel and efficient SF molecules necessitates solution processibility and high SF yield in the solid state. SF materials can be integrated with silicon or organic photovoltaics, most commonly as a thin film layer on top of the semiconducting material. These films can be inhomogeneous, consisting of different structural domains with different crystalline structures or degrees of crystallinity, making the study of SF in the solid state highly challenging. Morphological inhomogeneity may also disturb the local molecular or crystal symmetry, leading to potential changes in the SF mechanism. In this perspective, we analyse and combine approaches in both selecting model systems and using advanced spectroscopic methods to devise an approach to rigorously analyse SF materials in the solid state, with special emphasis on discussing how symmetry breaking (SB) processes such as formal charge transfer and SB vibrations can impact the key mechanistic steps of SF. From a material perspective, we critically discuss the advantages and drawbacks of using dimers/oligomers, nanoparticles, and aggregates as model systems, as well as methods for manipulating and controlling molecular stacking environments. Then, we provide a brief review of recent developments in advanced spectroscopic methods and the key findings of research relevant to SF in the solid state.

Received 1st November 2025
Accepted 20th March 2026

DOI: 10.1039/d5sc08452k

rsc.li/chemical-science

1 Introduction

Singlet fission (SF), first reported in solid-state anthracene in 1965,[1] has been widely investigated for its potential to support new advancements in photovoltaics,[2,3] quantum computing,[4] and elsewhere. In general terms, SF describes the process in which a single photo-excited singlet state (S_1) is used to produce two triplet excitons (T_1) of no more than half of the singlet energy. Since SF doubles the number of excitons in the system for a single photon absorption, it helps to overcome the over-band gap energy loss in photovoltaics when the triplet photon has energy greater than the bandgap of the semiconductor. At the best approximation, SF can improve the theoretical single-junction silicon solar cell efficiency to 42%.[5–7]

Efficient SF materials usually have the lowest singlet state energetically lying close to, or slightly higher than twice the lowest triplet state energy, and lower than the second triplet

School of Chemistry, The University of Melbourne, Parkville, VIC, 3010, Australia. E-mail: trevoras@unimelb.edu.au

Xinyue Xu

Xinyue Xu is a current PhD candidate in the Ultrafast and Microspectroscopy Laboratories at the University of Melbourne. Her project focuses on establishing and utilising advanced ultrafast transient absorption and transient vibrational spectroscopic experiments to study complex dynamics in singlet fission, photovoltaic, and photoswitching systems.

Christopher R. Hall

Dr Christopher R. Hall is an Australian Research Council Future Fellow at the University of Melbourne. He is interested in ultrafast spectroscopy (electronic and vibrational) applied to studying fast processes in molecular and biological switches, and semiconductors with applications in photovoltaics.

state (*i.e.* $E(S_1) \geq 2E(T_1)$ and $E(S_1) \leq E(T_2)$).[8–10] Systems that have $E(S_1) \leq 2E(T_1)$ such as tetracene, perylene, and their derivatives can undergo efficient endothermic SF; azulenes, thiones, and their derivatives have been demonstrated to undergo SF from higher singlet states in their molecular aggregates.[11]

However, satisfying energetic requirements does not guarantee efficient SF because the SF mechanism is system-dependent and may involve reversible steps and/or trap states. In brief, upon initial excitation, the chromophore in S_1 couples to another chromophore in the ground state. The coupled system forms a correlated triplet pair state (^{1}(TT)) with or without the involvement of a charge transfer (CT) state.[12–19] Eventually, in an ideal case, the ^{1}(TT) state forms a separated correlated triplet pair (^{1}(T$\cdots$T)) state from which spin coherence is lost to yield two triplet excitons which can then separate and diffuse apart. Ultimately, these excitons would be transferred to the active material in a photovoltaic device to generate a photocurrent.

Over the last 5 decades the field has developed an enhanced understanding of SF mechanisms, taking into account a broad range of conditions. This has generated a significant body of published work, which has been distilled into a number of key reviews. One of the first reviews by Smith and Michl (2010) provided insight into the mechanisms of SF and molecular design principles.[16] More recent synthetic, theoretical and spectroscopic advances (2015 – now) in the field have been summarised in numerous review and account articles.[8,9,20–29] To date, common methods for controlling SF efficiencies and mechanisms include; (1) tuning molecular structure and relative energies of states,[30,31] (2) controlling solvent interactions or matrix effects,[32–34] (3) magnetic field variation,[28] (4) temperature control,[35,36] (5) spatial arrangement of chromophores for example in dimers or oligomers,[37–39] and (6) morphology control in solid or colloidal states.[40–43]

Despite the large number of review and perspective articles, there are limited examples of a unified discussion of symmetry breaking (SB) and its importance to SF in the solid state.[9,21,22] Such discussion is pivotal as SF materials are most commonly integrated with devices in the solid state, where potential inhomogeneity (*e.g.* polymorphism or disorder) impacts molecular coupling orientations, hence, the local symmetry. It is known that SB is critical in all pathways of SF and is necessary for the formation of the ^{1}(TT) state. In the case where a formal CT state exists, SB is inherent as the charge distribution on the chromophore pair becomes asymmetric when the CT state is formed. The CT state is hence usually referred to as the SBCT state in literature. Materials that undergo indirect SF (such as terrylene-3,4 : 11,12-bis(dicarboximide) (TDI) derivatives[35,44,45] and 4,4-difluoro-4-bora-3a,4a-diaza-*s*-indacene (BODIPY) derivatives[46,47]) have well defined transient spectral signatures in the visible (VIS), to near infra-red (NIR) and mid infra-red (MIR) regions for SF intermediate states due to changes in excitation localisation and the molecular geometry. The SBCT state is especially interesting for dimer/oligomer systems and is more frequently studied in the solution phase, where the solvent plays an important role in tuning the relative energies of the SBCT and the ^{1}(TT) states.[32] SB is also important for the direct coupling of the S_1S_0 to the ^{1}(TT) state. The ^{1}(TT) state necessarily has a different symmetry than the S_1 state. Therefore, the mixing of these two states requires SB. For example, *ab initio* calculations have shown that the S_1S_0 and the ^{1}(TT) states in orthorhombic rubrene crystal (C_{2h} symmetry) have vanishing electronic coupling due to symmetry restrictions, and SF in such systems is driven by SB vibrations.[48,49] The vibrational coherence and SB vibrational modes in SF are typically studied by analysing the behaviour of the nuclear wave packets using two-dimensional electronic spectroscopy, time-resolved MIR and/or Raman techniques. Kim and Musser gave a comprehensive review on this topic in 2021.[20]

The current perspective explores the recent spectroscopic strategies toward studying and optimising solid-state SF materials. We will start with identifying key mechanistic steps and intermediates relevant to solid-state SF and briefly summarising the general experimental approaches for studying them. Special emphasis will be put on the importance of observing SB processes and how that is relevant to unveiling the SF mechanism. Some current experimental challenges will be presented and the systematic strategies for studying solid-state SF materials will be extensively discussed. In many cases, the transition from studying molecular systems in solution (homogeneous and controlled concentration) to the solid state is not without complications as inhomogeneity and local environment/geometry need to be considered. Several intermediate steps or alternative approaches (*e.g.* using dimers, trimers, aggregates or nanoparticles as model systems, or side-group designs) allow us to understand the impact of one or more geometric factors such as stacking distance and orientations. Then, we will explore the key techniques for directly probing SF and SB processes in both solution and solid states with more emphasis on the latter. Finally, future directions and opportunities for further enhancing the understanding of solid-state SF materials and devices will be proposed.

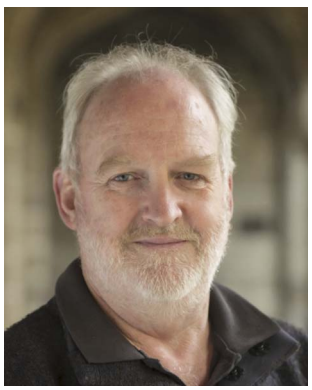

Trevor A. Smith

Trevor Smith is a Professor of Chemistry and leads the Ultrafast and Microspectroscopy Laboratories in the School of Chemistry at the University of Melbourne. He specialises in time-resolved spectroscopic techniques and optical microscopy methods for characterising light-driven processes in condensed phase materials.

2 Pathways of singlet fission

When discussing SF mechanisms, two fundamental questions need to be addressed: (1) is the pathway direct or indirect? (2) is SF coherent or incoherent? The first question can be addressed

by investigating the intermediate species involved. In a simple two-molecule and four-electron picture, initial excitation produces a localised excited S_1 state on one molecule with the other molecule in the ground S_0 state. The S_1 state and the S_0 state couple to form the S_1S_0 state. The direct mechanism describes the case where the correlated triplet pair state ^{1}(TT) is formed from the S_1S_0 state, whereas for the indirect mechanism, the formation of the ^{1}(TT) state is mediated by a real or virtual CT state (Fig. 1a). A real CT state is formed *via* a formal electron transfer step and can be observed experimentally. The second electron transfer step from the real CT state results in the ^{1}(TT) state. In the solution state, the presence of the real CT intermediate can be probed in a number of ways, including the solvent-dependent ^{1}(TT) formation kinetics and distinguishable transient spectral features, especially in the NIR region. High-polarity solvents tend to stabilize both the real and virtual CT states due to solvent dipole re-arrangement, and therefore facilitate the fast growth of ^{1}(TT) and triplet population.[32] In addition, the real CT state usually has different NIR excited-state absorption (ESA) features, which can be confirmed with transient absorprtion spectroscopy (TAS) data compared to the transient spectrum of the radical cation/anion pair upon one-electron oxidation/reduction. For SF mediated by a virtual CT state, the CT state is usually strongly mixed with the S_1 state, leading to ultrafast ^{1}(TT) formation (~100 fs – ps timescale); the transient characteristic ESA corresponding to the CT state can sometimes still be observed, providing proof for the virtual CT state involvement in the SF mechanism.[30,50] Furthermore, the process of CT formation is necessarily SB; however, in certain contexts, especially when disorder is present in the system, SB spectral characteristics can be extracted even with the direct SF mechanism.[51] This will be further discussed later in this perspective.

After the initial formation of the correlated triplet pair, the system may evolve to a number of states with different overall spin multiplicities, most commonly adopting overall $s = 0$ or $s = 2$ (Fig. 1a). Information on how species with different spin multiplicities evolve can be interrogated with transient electron paramagnetic resonance (trEPR) measurements,[52] as well as optical or vibrational spectroscopy.[53,54] The state represented by ^{1}(T···T) is a spatially separated triplet pair with the spin remaining correlated. In many cases, the direct observation of the ^{1}(T···T) is non-trivial and the ^{1}(TT) $\rightleftharpoons$ ^{1}(T···T) equilibrium dynamics cannot be extracted from time-resolved experiments due to the lack of spectral difference between these two states, and therefore, usually omitted in kinetic modelling. However, in systems such as TIPS-pentacene (TIPS = tri-isopropylsilylyl-ethynyl), the ^{1}(T···T) state has been distinguished from the ^{1}(TT) state in the VIS-NIR TAS experiment by examining subtle transient spectral variations.[53]

When there is strong electronic coupling between either the S_1S_0 state or the CT state with the ^{1}(TT) state, coherent SF occurs, and is marked by ultrafast ^{1}(TT) formation as well as sub-ps vibrational coherence probed with ultrafast vibrational spectroscopy[55] or 2D electronic spectroscopy.[45,56] In the regime of weak S_1S_0–^{1}(TT) coupling, the formation of ^{1}(TT) is relatively slow (> ps timescale) and is typically facilitated by SB vibrations, which changes the molecular geometry, and therefore, the overall symmetry to provide non-zero coupling between the S_1S_0 and the ^{1}(TT) states.[32,57] Another key experiment that can distinguish the incoherent and coherent mechanisms is temperature-dependent spectroscopy (based on emission or absorption), in which the ^{1}(TT) formation rate can be clearly tracked. Since the S_1S_0 – ^{1}(TT) process in an incoherent mechanism is non-adiabatic, barrier crossing rate constants typically follow Arrhenius-type behaviours.

In many cases, SF can proceed through a combination of the above-mentioned mechanisms. The direct and indirect, the coherent and incoherent pathways occur simultaneously, which greatly challenges the conclusive elucidation of SF pathways.[22,31,58] In addition, Monahan and Zhu addressed in an annual review, the critical role of CT character mixing or CT states in solid-state SF and the complications arising from exciton delocalisation.[12] The simplistic two-molecule and four-electron model is insufficient to describe all possible SF pathways and interactions. This presents challenges for both experimental and theoretical approaches to study SF in the solid-state. The mixing of CT states in direct SF mechanisms is

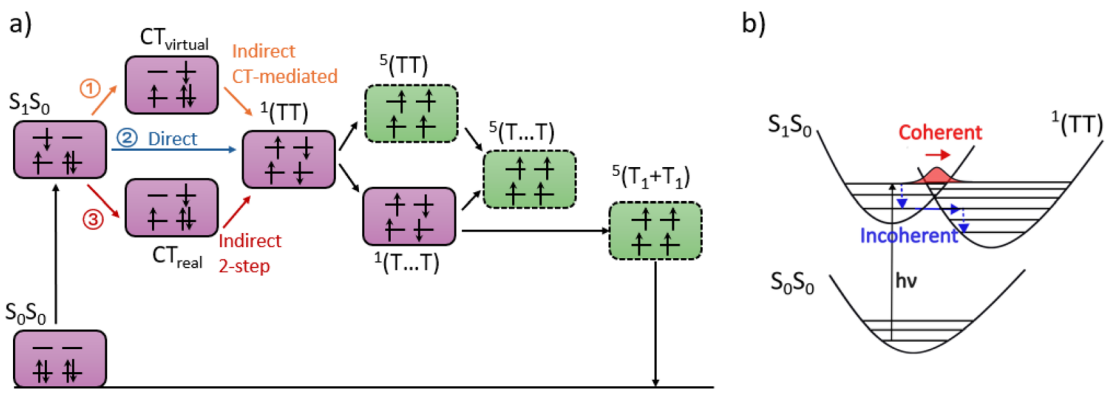

Fig. 1 Common SF pathways and mechanisms. (a) Pathways of SF and intermediate states; the states with net spin $s = 0$ are represented in purple boxes with solid outlines and those with net spin $s = 2$ are in green boxes with dashed outlines. Note that the placement of the states are not representations of their relative energies. (b) Coherent and incoherent SF mechanisms represented as an energy level diagram.

typically overlooked, especially in systems such as crystalline polyacenes where the commonly assumed mechanistic model only involves the correlated triplet pair states. The lack of evidence of the presence of CT states results in inconclusive mechanisms for many solid-state SF materials, and solvent polarity dependence cannot be employed as a tool for studying CT character. However, the SB nature of CT formation implies that time-resolved vibrational spectroscopy could provide evidence for such mechanisms.[59]

3 From solution phase to the solid state

A common practice for studying a new SF material is to first examine the material in solution to avoid the complexity introduced by the solid-state. However, the applications of SF materials in photovoltaics ultimately require studies in the solid-state. The translation to the solid-state leads to the introduction of a wide range of new structural features which are responsible for myriad competing excited-state processes. These include polarons, excimers, lattice vibrations, trap states and other intermolecular interactions arising from homogeneous and inhomogeneous packing and other morphological effects, such as grain boundaries. Some of these effects may be studied in isolation by the use of model compounds which emphasise a particular molecular structure and/or interaction. In the following section, we provide a brief discussion on several approaches to model such effects, including the design of packing orientation and intermolecular distance by linker or side-chain modification. We will also discuss some of these strategies in a broader context of studying SB. Then, we analyse several studies on nanoparticles, aggregates and self-assembly of SF materials and how these are relevant to progressing solution-phase SF study to solid-state SF studies. It is important to note that these discussions do not provide a full review of the respective field, but instead serve to illustrate key observations that aids the understanding of structural and symmetry effects on solid-state SF.

3.1 Dimers and oligomers as model systems

In dimer systems, consisting of two identical SF-capable monomers, the intermolecular distance, relative orientations, and degree of electronic coupling can be precisely controlled. In some cases, dimers can serve as models for SF studies in the solid state as they may represent similar inter-chromophore interactions to those in a crystalline or polymorphous environment.[25,62] Although computationally challenging, they are much simplified systems compared to bulk solids. Fig. 2 provides several examples of research in which understanding of dimer interactions may be invaluable for the study of conventional SF materials in the solid state.

In many SF systems such as polyacenes, coupling of two chromophores occurs through π–π interactions; the geometry of such interactions plays a critical role in the efficiency and the mechanism of SF.[58] Ahrens *et. al.*[38] synthesised and characterised nine novel spiro-linked azaarene dimers with various

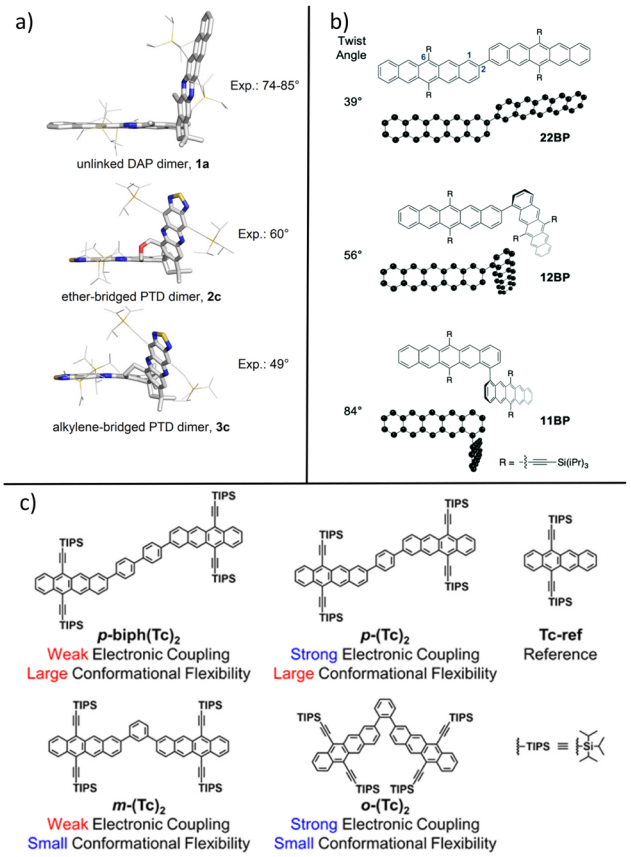

Fig. 2 Using dimers as model systems to study the effect of intermolecular packing arrangements. (a) Structures of spiro-linked dimers of DAP and PTD with different twist angles. Figure reprinted with permission from source.[38] Copyright American Chemical Society, 2021. (b) Structures of bipentacene dimers with varying twist angles Figure reprinted with permission from source.[60] Copyright The Royal Society of Chemistry, 2021. (c) Chemical structures of planar tetracene dimers used in the referenced study. Figure reprinted with permission from source.[61] Copyright American Chemical Society, 2021.

linkers to tune the angle and distance between chromophores and thereby the π–π interactions (Fig. 2a). The phenazinothiadiazole-dimers (PTD) achieved SF efficiencies near 200% in solution and the variations in SF yields have relatively small dependence on the twist angle. The diazapentacene-dimers (DAP) and tetraazapentacene-dimers (TAP) both exhibited twist-angle-dependent SF efficiencies with highest efficiencies achieved with twist angles ∼ 47°. TAS kinetics revealed that the rate of ^{1}(TT) formation was positively affected by the lower twist angle, which increases the π orbital overlap necessary for this step. Linker flexibility has a negative impact on the ^{1}(TT) formation rate, likely due to the large number of possible conformations, with only some having favourable equilibrium geometry for forming the correlated triplet pair state. The branching ratio improves with decreasing twist angle, especially with the DAP series, showing that in these rigid spiro-linked dimers, the increased orbital overlap not only promotes the formation, but also facilitates the decorrelation of triplet species. Many other studies[60,63,64] also explore the effect of

coupling angles in a dimer environment. While the molecules are in solution, the pair–wise interactions always have a well-defined rigid geometry, which serves as a good step for studying such chromophores in a more complex solid environment where one or more pair–wise coupling orientations may be present due to inhomogeneity.

Yablon *et. al.*[60] used bi-pentacene chromophores with varying twist angles to examine the effect of inter-chromophore coupling orientations on the triplet pair recombination in the solution phase (Fig. 2b). The authors employed optical TAS and computational calculations to show that by increasing the inter-planar twist angle from 39° (22BP) to 84° (11BP), the timescale of ^{1}(TT) formation slowed from 0.79 ps to 7.1 ps but the lifetime of the correlated triplet pair increases from 0.45 ns to 29 ns. The repopulation of the S_1 state was shown to be temperature independent and proceeds through a radiationless multiexciton internal conversion pathway. Their study was valuable to demonstrate the increased dihedral inter-chromophore coupling angle leads to slowed ^{1}(TT) formation rate but with favourable compensation due to ~50 fold increase in ^{1}(TT) lifetime.

The dependence of SF rates and efficiencies on molecular stacking and orientations is highly system-specific, and the study with dimers should be treated with care. Sometimes, additional complexity can be inherent in a dimer model, leading to a more complex interpretation of the mechanisms, where inter-molecular and intra-molecular SF can both occur. One big factor is that dimers in solutions behave nonstatically, meaning that they have rotations or vibrational motions during the SF process which a coupled pair in the solid system might not possess. For example, the covalently linked TIPS-pentacene derivative dimers presented by Kim *et al.* show heterogeneous SF in solution, that is, a single wavelength excitation or a single ensemble of rate constants is insufficient to describe the dynamics of the system with a broad distribution of conformers.[65] When the same dimers were cast as thin films, the dynamics were much more simple. Structural fluctuations can have tuning effects on the efficiency of SF; the goal is to strike a balance between electronic coupling and establishing a potential energy surface favourable for triplet separation.[61,66,67] Fig. 2c) shows a systematic study by Nakamura *et. al.*, introducing a highly efficient SF dimer based on tetracene. The *p*-biph(Tc)$_2$ dimer, which has a SF quantum yield close to 200% in solution, exhibits a planar structure in the electronic ground state, whereas the geometries in the singlet and the quintet (before triplet separation) states are twisted. In this study, where the SF chromophores are based on tetracene, the requirement of inter-chromophore coupling geometries through conformational flexibility to achieve efficient SF is again different from solid-state SF interactions. Although the authors did not further investigate these dimers in the solid state, the differences in SF kinetics between the dimers could be reduced due to structural planarisation and conformation restrictions. Additionally, both inter-molecular and intra-molecular coupling SF pathways should be considered given the Tc backbone allows for π–π stacking interactions, leading to potentially challenging investigations for these systems in the solid-state environment.

SB processes, which are essential to SF, are also frequently explored in the context of dimer systems in solution.[44,68–70] The tuning of dimer geometries will usually result in the tuning of SF pathways and the role of CT states in the overall mechanism. For example, Marguiles *et. al.* studied a series of stacked terrylenediimide (TDI) dimers with different degrees of slipping.[37] As the slip angle decreases, the excited-state kinetics became increasingly solvent-dependent, together with the observation of the characteristic CT TAS signal, and the stronger dominance of the SBCT state in the SF mechanism was clarified. In another important study, Alvertis *et. al.* exploited the role of SB vibrations and solvent interactions with a dimeric molecule in tuning the mechanism of SF (Fig. 3).[32] The well-defined symmetry of a dimer is crucial for allowing computational calculations on both the vibrational modes and the specific solvent–environmental interactions.[33] In non-polar solvents, SF mostly proceeds through formal CT states, however, increasing solvent polarity brings the CT state within energetic proximity to the ^{1}(TT) state, allowing mixing *via* a torsional motion along the connective bond between monomer units (Fig. 3a and d). The approximate C_2 symmetry puts a constraint on the SF mechanism. Through computational calculations, the ground TT state is a quintet instead of a singlet state, and is *A*-symmetric. The dihedral rotation Φ has the same *A* symmetry, whereas the optically accessible localised excitonic (LE$_B$) and CT$_B$ states are *B*-symmetric. The formation of the TT state must be achieved with some form of SB. In intermediate polarity solvents, SB is provided by solvent interactions. However, in the low-polarity solvents, without generating additional *B*-symmetric vibrations, excess excitation energy leads to hot-state vibrations and large displacement along the Φ coordinate, allowing for transition through avoided crossing at large torsion angles. Similar concepts for tuning SF pathways with solvent were explored in spiro-fused TDI dimers using temperature control,[35] and measures for tuning CT characteristics *via*

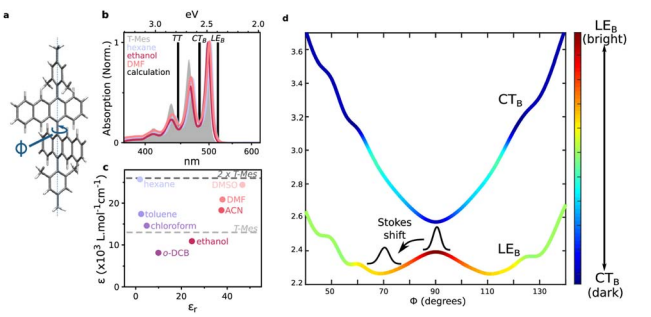

Fig. 3 (a) Chemical structure of the dimer of T-Mes in the referenced study indicating the torsional motion involved in CT/^{1}(TT) mixing. (b) Ground-state absorption spectra of the dimer in different solvents. (c) Peak molar extinction coefficient of dimer in various solvents compared to that of the monomer in chloroform (dashed). (d) Potential energy surfaces of the two bright excited states along the torsional coordinate. The colour code indicates the mixing between the LE$_B$ and CT$_B$ surfaces, leading to finite oscillator strength for the latter through intensity borrowing. Figure reprinted with permission from source.[32] Copyright American Chemical Society, 2019.

connectivity tuning have been explored in many publications.[66,70–74]

Moving towards our goal of understanding SF in bulk materials with potential heterogeneity, adding monomeric units to the system to form trimers and larger oligomers or ordered polymers would offer potentially useful insights.[25,39,75,76] However, careful considerations must be taken when comparing results from a dimer/oligomer model system to those of a bulk solid. Several questions need to be asked and addressed: (1) Will the excited state dimer undergo geometric change, if so, by restricting the geometric distortion (either with increased viscosity, functional group substitution, or decreased temperature), how will the excited state dynamics change?; (2) What is the suitable choice of solvent for the system to perform optical experiments in, that is, to carefully consider the role of solvent in the SF mechanism?; (3) How does the geometry compare to the pair–wise interactions in the crystal environment, and do more than one arrangement need to be considered? (4) Does the linker in the dimer system provide additional electronic coupling that may not be present in a solid-state environment of the unlinked monomers?

3.2 Nanoparticles and aggregates

Aqueous colloidal nanoparticles of many SF materials can be readily prepared by re-precipitation, and often retain their SF properties but with different dynamics when in solution or in bulk solids.[2,40,77] Compared to dimers or oligomers in the solution phase, nanoparticles may be more representative of the solid material and allow for the examination of; (1) charge transfer interactions,[78] (2) exciton delocalisation, (3) molecular packing effects,[79] and (4) surface effects.[80,81] In addition, using aqueous suspensions of nanoparticles can reduce certain undesirable effects such as optical scattering and strong polarisation-dependence associated with performing spectroscopy on crystalline materials. Pensack *et. al.* synthesised two types of TIPS-pentacene nanoparticles (I and II, diameter 70–80 nm) with structural and optical properties similar to those of amorphous and crystalline films, respectively.[43] The SF behaviours of these nanoparticles studied in solution resemble that in the bulk solids, with the more crystalline particles undergoing efficient SF, and the more amorphous particles suffering from losses of triplet population after formation of the ^{1}(TT) state. The authors attributed this loss to a statistical distribution of packing arrangements in the material, leading to undesirable charge recombination prior to triplet separation. They then characterised the initial ^{1}(TT) formation efficiency for both the amorphous and crystalline TIPS-Pn NPs to be almost 100%, but the time-constant for ^{1}(TT) formation is 10 fold slower in the amorphous NPs. Additionally, mixed morphology nanoparticles were also successfully synthesised to show that neither singlet nor triplet excitons migrate between the amorphous and crystalline domains. However, when studying nanoparticles, the size effect must be considered. Hudson *et. al.* used amorphous TIPS-pentacene nanoparticles in the size range of 30–80 nm as a model system and provided insights on why discrepancies may exist between measurements of nanoparticles and bulk solids.[40] The authors identified three primary exciton decay pathways in the nanoparticle system (Fig. 4c): (1) non-radiative singlet decay with rate constant k_{NR}, (2) non-radiative triplet pair decay with rate k_{pair} and (3) geminate recombination from separated triplet pairs with a rate constant of k_T. Optical TAS data show that small nanoparticles have significantly reduced triplet lifetimes and slower ^{1}(TT) growth compared to larger particles (Fig. 4a and b). They identified that the reduced particle diameter leads to greater structural disorder, promoting fast geminate TTA, and the fractional population undergoing non-radiative singlet decay has negative correlation to particle sizes. At a particle size of 80 nm, the properties of the nanoparticles approach that of a bulk solid, which is in agreement with the investigation by Pensack *et. al.*

Aggregates typically have well-defined stacking geometries and their dipole orientations can be characterised with steady state absorption spectroscopy based on spectral splitting and shifts. They can mimic the behaviour of a small segment of an ordered bulk solid, or one single domain in a polycrystalline film.[82] In some cases, by understanding whether aggregation would favour SF, pre-aggregation before casting films could be implemented to maximise solid-state SF yield. Wang *et. al.* reported highly efficient SF in H-type aggregation of the dipyrrolonaphthyridinedione (DPND) molecule.[83] They found that the aggregate has a significantly stabilised CT state, which is energetically close to the excimer trap states. This results in state character mixing and assists the trapped population to further evolve to the correlated triplet pair state; from there, triplet separation can occur, which is highly unusual in SF systems. In addition, aggregates can be used in conjunction with microcavities to study the exciton–polariton interactions in SF systems.[84,85]

To briefly summarise, nanoparticles and aggregates allow us to examine SF in a close-to-solid-state packing arrangement while maintaining the opportunities to perform measurements

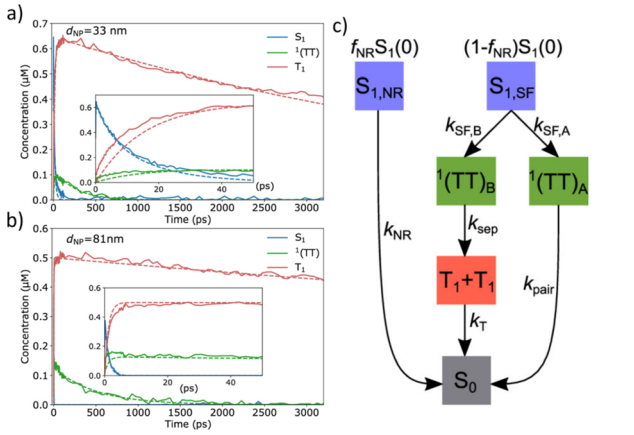

Fig. 4 The particle size effect on SF for amorphous TIP-Pn nanoparticles studied in solution. The population evolution of $S_1$1(TT) and T_1 states obtained from ultrafast TAS experiments for (a) 33 nm and (b) 81 nm particle sizes (c) the kinetic scheme used to analyse the TAS data. Figure adapted from source[40] with permission. Copyright American Chemical Society, 2021.

where a solvent is required or solvent interaction could be useful to identify mechanistic steps. In some cases, nanoparticles and aggregates have more well-defined or tuneable morphology compared to the bulk solid. However, where possible, comparison against solid-state samples should be made to identify any discrepancy due to size, or surface effects.

3.3 Substituents and crystal formation conditions

For common SF materials such as polyacenes, the molecular stacking arrangement in the solid state can be precisely tuned by side-chain engineering as well as carefully controlling the film formation conditions. Mayonado *et. al.* used functionalised derivatives of fluorinated anthradithiophene diF R-ADT (R = TES, TSBS, TDMS, TBDMS, see Fig. 5 a for the structures) and prepared single crystals for their analysis using polarisation-dependent transient absorption microscopy (TAM).[86] Fig. 5a shows that the four substituents resulted in three distinct packing arrangements, and each differs mechanistically during SF, and exhibits structure-dependent ^{1}(TT) formation efficiencies. The TES-substituted brickwork crystal has almost unity ^{1}(TT) formation efficiency, the TDMS, and TBDMS substituted structures have around 85% efficiency, whereas all excited state population in the sandwich herringbone structured crystal falls into a CT-type self-trapped excitonic state due to lack of symmetry in the crystal environment. Further discussion on the spectroscopic techniques implemented will be provided in a later section of the perspective. The work by Margulies *et. al.*[31] also explored the substituent effect of pair–wise geometries in polycrystalline thin films of tetracene-derivatives with various degrees of slipping in molecular stacking on SF rate parameters and mechanisms. Their study revealed that SF yields positively

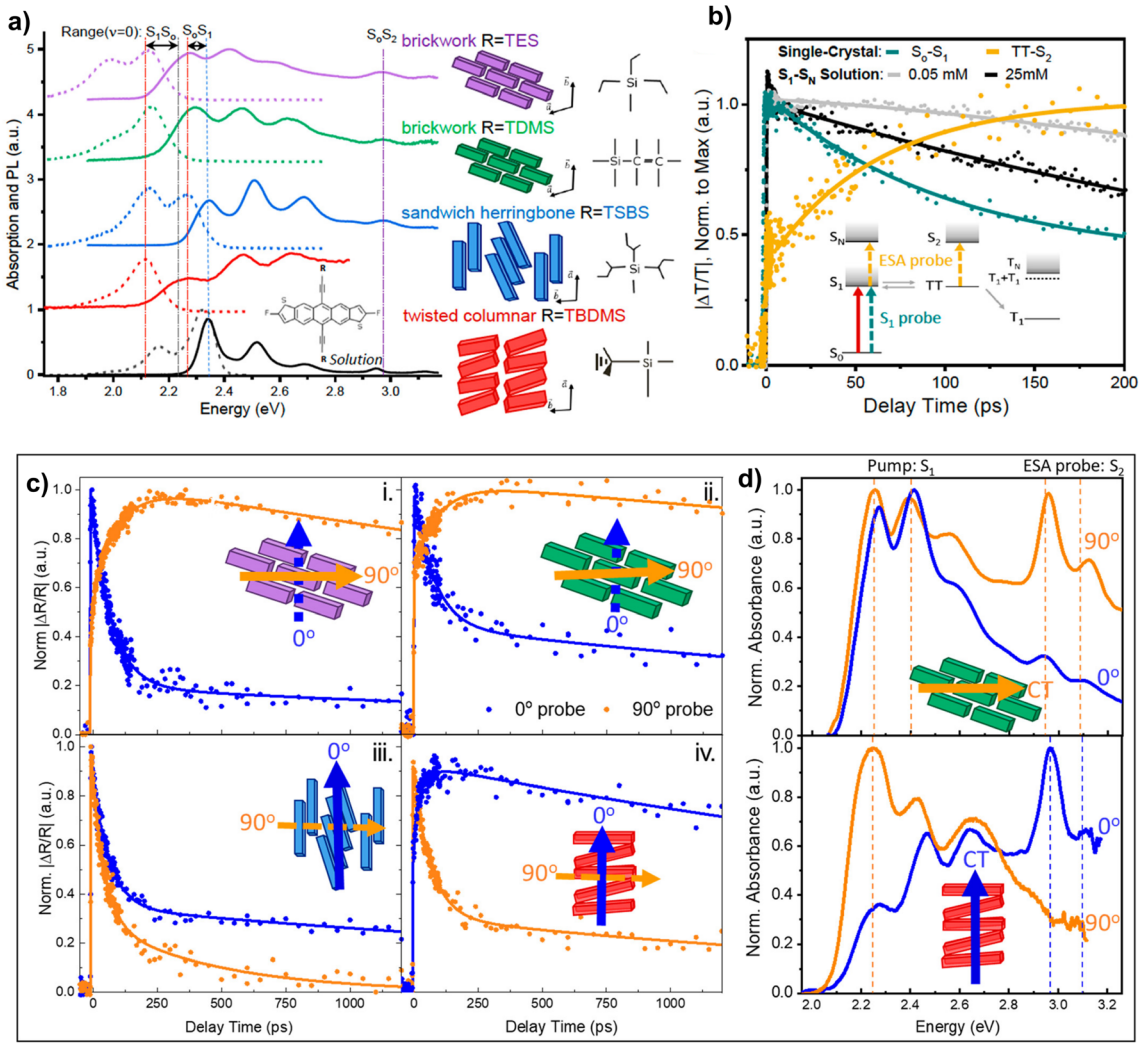

Fig. 5 Side-chain design controls the crystal packing structure and SF mechanism (a) absorption (solid lines) and emission (dashed lines) of diF R-ADT derivative single crystals and solution steady-state spectra in black lines, the representations of crystal packing structures are also shown (b) TAM results of diF TES-ADT crystal following 2.3 eV pump pulse (the yellow kinetic trace is the probe for ESA of the ^{1}(TT) state and the green line is the GSB feature of the S_1 state solution S_1 decay kinetics are shown in black and grey at 25 mM and 0.05 mM concentrations, respectively). (c) TAM kinetics obtained for all crystals probed in the NIR region 1–1.4 eV with polarisation parallel (blue) and perpendicular (orange) to the crystal axis (d) the absorption spectrum of the TDMS and the TBDMS derivative with probe polarisation parallel and perpendicular to the crystal axis in blue and orange, respectively. Figure adapted with permission from source.[86] Copyright American Chemical Society, 2022.

correlate to the degree of slipping in the stacked chromophores and the degree of π orbital overlap does not necessarily determine the SF efficiency in such systems. The intermolecular distance can also be tuned by substitution.[87] For example, by selectively substituting carbon atoms in the aromatic backbone of TIPS-pentacene with nitrogen, the packing distance can be decreased by 2%, resulting in an enhanced SF yield. The electronic effects of side-chain substituents should be considered carefully if the desired outcome of the study is to isolate the effect of stacking geometries. These effects can usually be studied with solution-phase characterisations, steady-state optical spectroscopy and or electrochemical studies, as well as computational chemistry.[61,88,89]

Controlled film preparation (thermal/solvent vapour annealing) or single crystal growth can also offer solid-state samples with relatively well-defined chromophore stacking geometries. The common SF material TIPS-pentacene can be cast into pure amorphous, Type-II brickwork structure crystalline films, or polycrystalline films under no-annealing, solvent vapour annealing, and thermal annealing conditions, respectively.[90] However, the amorphous film is usually prone to laser-induced heating, which causes local thermal annealing.[91,92] Single crystals of rubrene[58] or tetracene derivatives[56] can be prepared with well-defined crystal structure, but for certain materials such as TIPS-anthracene and TIPS-tetracene, polymorphism is usually unavoidable in spin-cast thin film samples.[93] For these materials, local inhomogeneities may still present great challenges to the interpretation of results from spectroscopic experiments. Techniques such as Raman mapping can also be useful for identifying local morphologies. However, sample damage is a common drawback of this technique.[94]

4 Spectroscopic strategies for observing singlet fission and symmetry breaking

Optical and magnetic spectroscopic techniques such as TAS, time-resolved photoluminescence (TRPL), and trEPR play a crucial role in the study of SF materials. These techniques are mostly readily accessed and considered "standard practice" in assessing SF efficiencies, rates and mechanisms both in the solution phase and the solid state. The vis-NIR region has been used to identify intermediates and final products of SF[53,95] especially states with significant CT character, which can manifest as broad features spanning the lower energy visible to NIR spectral range, matching the absorption spectra of the radical ion pairs.[22,37,96] For materials that undergo coherent SF through correlated triplet pair states, and perhaps a mixture of coherent and incoherent mechanisms, the large number of possible decay pathways and intermediate states may result in complex kinetic models with a large number of kinetic parameters. Performing global analysis on TAS or TRPL data sets with these kinetic models may be convoluted and potentially unreliable. This is because the electronic absorption features in the vis-NIR region are usually broad, with overlapping ground state bleach (GSB) and ESA features.[97] In certain systems, the study of vibrational signatures using MIR transient absorption spectroscopy,[51,98] time-resolved Raman spectroscopy,[99] or multidimensional spectroscopy[20,100] will aid the extraction of unique vibrational signatures of intermediates. Since the oscillator strengths of vibrational modes are also highly symmetry-dependent, these measurements will also provide insights on the transient local symmetry with the aid of computational calculations. In the past five years, emerging studies have employed time-resolved microscopy to study solid-state SF materials, focusing on the local packing environment and crystalline domains.[92,101–105] In this section, using recent studies employing the techniques mentioned above as examples, we provide discussions of the considerations to be made when applying different spectroscopic techniques to solid-state SF systems. In addition, we identify potential artifacts when analysing optical and vibrational spectroscopic data, for example, spectral shifts due to laser-induced heating and local annealing; these should be carefully distinguished from real SF intermediates.

4.1 Transient electron paramagnetic resonance spectroscopy

TrEPR spectroscopy, or transient electron spin resonance (trESR) spectroscopy is a powerful technique in distinguishing SF intermediates with different spin characteristics. The principles and applications of this technique in a broader context can be found in other literature[107,108] and here we summarise some recent advances of this technique in the field of SF studies and analyse its advantages and limitations.

TrEPR has a typical time-resolution on the order of 10 s of ns to ~μs, therefore, for a SF system to be studied with this technique, the correlated triplet pair states must evolve on comparable timescales. If this requirement is satisfied, trEPR can complement optical TAS data on shorter timescales to unequivocally assign triplet pair states with singlet, triplet or quintet multiplicities and potentially distinguish triplet populations formed from triplet pair separation from those formed from ISC if these processes occur on different timescales or *via* intermediate states with different spins.[109] Additionally, the development in data analysis allows for the simulation of experimental trEPR spectra based on system evolution dynamics and expected spin states using open-source packages.[110] In recent years, several studies have elucidated the impact of molecular coupling in dimers and oligomers on triplet pair separation pathways.[111–113] Dill *et al.* used X-band trEPR spectroscopy to study the intra-molecular SF dynamics in a rigid TIPS-bipentacene dimer immobilised in a dilute glass matrix. The authors demonstrated that certain ^{5}(TT) state sublevels were selectively formed after formation of ^{1}(TT) because of the alignment of the key magnetic axes due to dimer rigidity. Their work provides molecular design guidelines for the application of SF in quantum computing.[113]

TrEPR is also commonly employed to study solid-state SF materials to reveal packing-structure-induced changes in SF dynamics.[106,109,114,115] Bu Ali *et al.* used a combination of

temperature-, fluence-, and magnetic field-dependent PL measurements complemented with trEPR results to show the temperature-dependent formation of the ^{1}(TT) state in drop-cast crystalline 2,8-difluoro-5,11-bis(triethylsilylethynyl) anthradithiophene (diF-TES-ADT) films. Fig. 6a) shows that as the temperature increases from 40 to 250 K, the spin polarisation changes from a symmetric eeaaa pattern (corresponding to the triplet) to an almost emissive-spin-polarisation-only pattern. The triplet feature decreases in intensity as the temperature increases and a narrow emissive feature at 348 mT suggests the formation of a spin-correlated radical pair formed by ISC and, or TTA. The fluence-dependent trEPR at 100 K showed that the delayed net emissive spin polarisation follows the TTA kinetics, and combined with the kinetic data from TRPL studies, the kinetic model in Fig. 6 was devised. The authors proposed that at temperatures below 270 K, ISC from ^{1}(TT) to the triplet state dominates over triplet pair separation.[106] Phase-inverted echo-amplitude detected nutation (PEANUT) is a pulsed EPR technique that probes the Rabi oscillations (or nutation) to distinguish the spin states of paramagnetic species. Macdonald *et. al.* have used this technique to identify anisotropic ^{3}(TT) generation and distinguished ^{5}(TT) states generated *via* two separate mechanisms enabled by different time-dependent spin exchange energy fluctuations in a SF tetracene hetero-dimer.[116]

Combined with optical characterisation, trEPR is extremely powerful in probing the evolution of spin characteristics in the system at a longer time scale. However, the following limitations must be considered when employing this technique. (1) Ultrafast formation and separation of the correlated triplet pair states (*e.g.* in crystalline TIPS-Pn and rubrene) do not occur on the timescale probeable by trEPR; (2) if the two triplets have very strong exchange coupling (*i.e.* J ≫ microwave frequency), the ^{1}(TT) state will appear EPR-dark and the quintet features are likely suppressed; (3) structural disorder and polymorphism broadens trEPR signals, resulting in challenging interpretation of data and ambiguity in the assignment of states; (4) systems with fast spin relaxation (*e.g.* due to heavy atom effect) or low SF yield will likely suffer low signal in trEPR; (5) trEPR experiments often require the sample to be measured at low temperatures in a frozen matrix using quite high laser fluences (~mJ cm^{-2}), meaning sample degradation must be considered under such conditions.

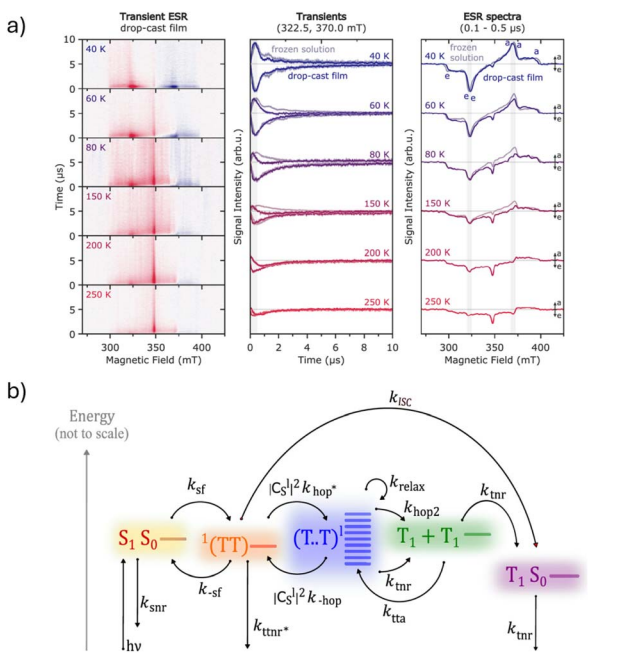

Fig. 6 trEPR study of diF-TES-ADT drop-cast films. (a) trEPR measurements on diF-TES-ADT drop-cast films at a range of temperatures; from left to right are the 2D colour map of the trEPR data, the kinetic traces at 322.5 mT and 370 mT, and the spectra at 0.1–0.5 µs. (b) The kinetic scheme for the SF and ISC of diF-TES-ADT drop-cast films. Figure adapted with permission from source.[106] Copyright American Chemical Society, 2025.

4.2 Optical spectroscopy and microscopy

Thin film characterisation is an important part of studying solid-state SF materials. However, traditional film preparation such as spin-coating and doctor blading may result in polymorphous films that cannot be completely circumvented by annealing. Studying SF dynamics in polymorphous systems can be challenging due to the presence of inhomogeneity, which may further complicate exciton dynamics, and in such cases, kinetic analysis needs to be performed rigorously and with care. De Clerq *et al.* recently used a combination of TAS, magnetic field-dependent PL and time-correlated single photon counting (TCSPC) to explain the loss mechanisms in mostly amorphous (mixed with a polymorph, characterised by steady-state absorption (Fig. 7b) and X-ray diffraction), low–SF-yield TIPS-anthracene thin films.[93] Their work provided compelling evidence that the main loss pathway is *via* direct internal conversion (IC) in the S_0 or ^{1}(TT) manifold instead of the previously proposed intersystem crossing (ISC) to higher triplet states (Fig. 7a) observed in acenothiophene.[117] In addition, they demonstrate the powerful method of globally analysing data from different experiments targeted to a specific kinetic model to extrapolate kinetic rate parameters.

In their study, TAS was conducted in both the solution phase (no SF expected) and the solid state. The decay of the GSB at 450 nm into an ESA is evidence of intermediate species associated with SF. The presence of triplets at longer time was confirmed by photo-sensitisation studies. Upon close examination of the decay-associated spectra (DAS) of the sequential best-fit with the least number of components (three exponentials), the second component from the sequential model still exhibits significant S_1 character (ESA at 535 nm), suggesting that a quasi-equilibrium exists in the first step (Fig. 7c). Therefore, the kinetic model was adapted to extract clean S_1S_0, ^{1}(TT), and T_1 transient spectra (A, B, and C, respectively in Fig. 7d). To further characterise the intermediate species, a magnetic field was applied to hinder the formation of free triplets. Fig. 7e) shows the PL with applied magnetic field and for TIPS-anthracene, the increase is very small, corresponding to low SF QY, and the TCSPC results (Fig. 7f) show that the majority of population decays with a 115 ps time constant.

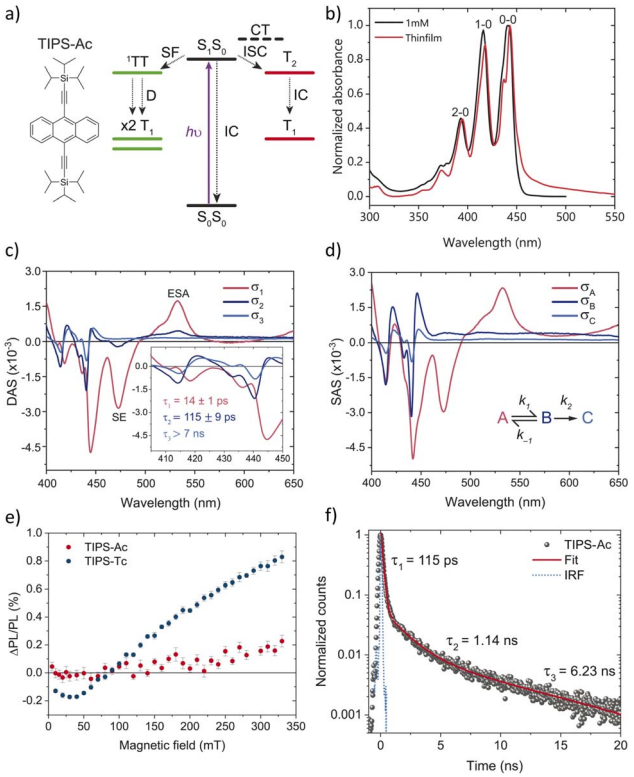

Fig. 7 The SF study on polycrystalline TIPS-Ac film (a) the chemical structure of TIPS-Ac and the SF scheme. (b) The steady-state absorption spectra of solution and thin-film TIPS-Ac showing vibronic progression. (c) DAS obtained with the TAS (380 nm excitation) data analysed with sequential three-state model. (d) The SAS obtained with the model shown in the inset. (e) Magnetic PL data of TIPS-Ac thin film compared to TIPS-Tc thin film. (f) TCSPC data obtained with 405 nm excitation, emission collected after 450 nm short-pass filter. Figure adapted from source[93] with permission. Copyright The Royal Society of Chemistry, 2024.

Two models, one with IC of the singlet spin states as the major decay pathway and the second with ISC to a higher triplet were used to model the magnetic PL and TAS results. It was found that both results can be reproduced by kinetic modelling without introducing higher triplet states, and the triplet yield produced by the model was also in agreement with experiments, allowing for the conclusion that IC is the dominant loss mechanism. In the TIPS-anthracene thin films, the presence of excimers was evident in the long tail of the absorption feature beyond 500 nm, but the role of excimers (frequently acting as trap states of SF) was not explicit; no direct evidence indicated that they are involved in the process of SF. TRPL studies in solid-state systems should be treated with extreme care as in some cases, PL signals may originate from both the excimer and the ^{1}(TT) state *via* Herzberg–Teller coupling, where electronic transitions mix with vibrational modes upon SB.[95] This emissive triplet pair state was reported for a range of systems including pentacene crystals and anthradithiophene pure and blended thin films.[95,118,119]

The study of single crystals is also of pivotal importance to solid-state SF characterisation. In such systems, well-defined crystal axes offer the opportunity to explore polarisation-dependent exciton dynamics and transient spectral evolution. Time-resolved microspectroscopy (*e.g.* TAM) with polarisation dependence can be employed to differentiate SF intermediate states with different spectral features and transition dipole orientations. Additionally, the spatial resolution offered by TAM allows for identifying kinetic differences at the crystal edges or defects compared to the bulk, hence, explicating the impact of inhomogeneity and local SB on SF dynamics.

In the previous section, we have introduced the work by Mayonado *et. al.*[86] Exploiting the distinct transition dipole orientations of various SF intermediates, the authors directly probed SF dynamics parallel and perpendicular to the crystal axes and explained the effects of packing arrangements on SF mechanisms. Calculations showed that the CT transition dipoles or the brickwork and the twisted columnar structures are aligned with the $S_2 \leftarrow S_0$ transitions (perpendicular and parallel to the crystal axis, respectively). This was further confirmed by absorption spectra probed along and orthogonal to the crystal axes (Fig. 5d). Polarisation-dependent TAM showed packing-structure-dependent ESA dynamics in the 1–1.45 eV region where the dominant signal arises from either $S_n \leftarrow S_1$ or $S_2 \leftarrow ^1$(TT) transitions (Fig. 5c). The rise in ESA signal when probed along the CT axis (TT formation) can be fitted with comparable rate constants to the falling dynamics of S_1 when probed with the orthogonal polarisation. This allows for assigning a CT-mediated SF mechanism with the TT formation efficiency estimated by the ratio between the rising and falling rate constants. For the more disordered sandwich herringbone structure, only falling kinetic behaviour was observed (Fig. 5c (iii)). This observation was rationalised by a CT-mediated self-trapping mechanism owing to lower symmetry of the crystal structure.

A series of works by Zanni's group highlighted the effect of local packing environment in SF material single crystals on the rate of triplet pair and triplet formation. In the study of TIPS-pentacene microcrystals by Jones *et. al.*,[103] 2D white light spectroscopy with visible, orthogonally polarised pump and probe beams, and spatial resolution less than 1 μm resolution was employed. With this approach they found that non-equilibrium stacking structures at the crystal edges facilitate enhanced triplet formation by allowing population exchange between the singlet and triplet species. Similar findings were made by Armstrong *et. al.*[92] for TIPS-pentacene thin films, where structural defects or slip-stacked disordered structures led to higher SF yields. A more recent study by Volek *et. al.* with orthorhombic rubrene crystals provides further evidence on locally broken symmetry enhanced SF.[101] Steady-state absorption and PL spectra (Fig. 8a) show broadened vibronic peaks and red-shifted emission at the crystal edge, indicating an ensemble of packing structure with different pair-wise geometries. The findings were corroborated by PL and Raman mapping (Fig. 8b and c). TAM images taken at 20 ps and triplet population kinetics at 515 nm probe wavelength (Fig. 8e and f) provide direct evidence for faster triplet formation near crystal edges with an approximately 4-fold increase in rate constants compared to the bulk of the crystal. The results by Zanni's group are in line with earlier

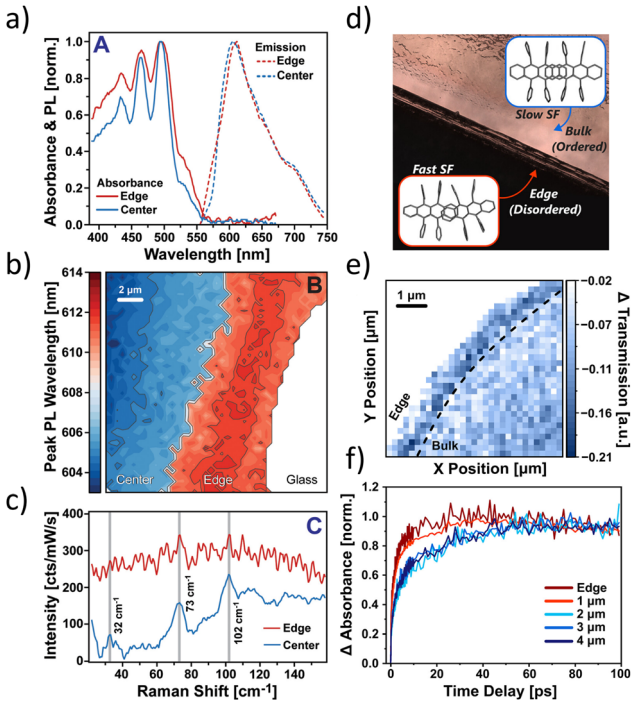

Fig. 8 TAM investigation on the effect of structural disorder on SF in rubrene single crystal. (a) Steady-state absorption and emission spectra in the centre and the edge of rubrene crystals. (b) PL peak emission wavelength map (c) Raman spectra at the centre and the edge of the crystal (d) Illustration of molecular orientations at the edge and the centre of the crystal (e) TAM mapping of the rubrene crystal detected with pump and probe wavlengths of 535 nm and 510 nm at a delay of 20 ps, the probe wavelength reflects the ESA of the T_1 state. (f) The TAM kinetic traces taken at different distances from the edge of the crystal. Figure adapted with permission from source.[101] Copyright American Chemical Society, 2023.

theoretical research by Petelenz and Mateusz,[120] where the authors identified that existing SB or lowered symmetry at crystal edges and defects increases the coupling between the singlet and the triplet pair state, hence, enhances SF.

The direct observation of spatial variations in morphology and SF rates offered by TAM is extremely powerful, as spatially localised ultrafast spectroscopy can also be used to disentangle the contribution of coherent and incoherent SF pathways. Liu *et. al.*[58] exploited micro-area fsTAS with temperature-dependent measurements to characterise SF pathways in monoclinic, triclinic and orthorhombic rubrene crystals. The ^{1}(TT) formation kinetics were tracked with a characteristic ESA band in the visible region. The monoclinic crystal exhibited single-exponential ^{1}(TT) rise kinetics with a time constant of 24 ps, consistent with an incoherent SF mechanism. Both the triclinic and orthorhombic crystals showed bi-exponential ^{1}(TT) decay that involves a much faster component, suggesting a mixture of coherent and incoherent mechanisms. The temperature-dependent kinetics showed Arrehnius-type behaviour for both crystals between 80 K and 298 K. Simplified dimer models were used to calculate electronic couplings between pair–wise interactions. Symmetry restrictions resulted in negligible S_1–^{1}(TT) coupling, therefore, the mechanism was proposed to be CT-mediated, with 35% and 45% coherent mixing for the ortho and triclinic crystals, respectively. The above-mentioned studies do not investigate the effects of local morphology on triplet separation and transport, which is also crucial for determining the final SF yield. Berghuis *et. al.* used diffraction limited time-resolved microspectroscopy (TRMS) including TAM and time-resolved emission microspectroscopy (TREM) to study triplet diffusion in single crystals of tetracene.[102] However, their study did not include systematic analysis of the effect of local packing environments.

4.3 Vibrational spectroscopy

Due to the sensitivity of IR vibrational modes to symmetry, ultrafast TAS experiments with mid-IR probe (TRIR) have been frequently used to explore SBCT processes in donor–acceptor materials[121–124] or other photovoltaic systems including SF materials.[22,44,99] When the SF system proceeds through a formal CT state, where the symmetry is broken, new IR modes are expected and additional ESA peaks should be present in the transient spectra. For pair–wise interactions, the transient species will have similar absorption features to that of a radical ion pair.[22] In the solid-state, the oscillator strengths of IR active modes are not only governed by the molecular symmetry, but also crystal symmetry. SB can occur in the excited state through SB vibrations or interactions with the surrounding environment.

The series of works by Grieco *et. al.*[54,90,91] highlights the importance of TRIR in analysing solid-state SF of TIPS-Pn.[125] The anti-symmetric alkyne stretch of the TIPS functional group at 2120 cm^{-1} in ground-state crystalline TIPS-Pn thin films (Fig. 9a and c) has a corresponding triplet vibrational mode 10 cm^{-1} to lower wavenumbers. By fitting TRIR data with skewed Lorentzian functions at the singlet and the triplet vibrational resonance energies, the coherent SF mechanism and rate parameters were extracted (Fig. 9d). The further advancement of their work in 2019 (ref. 51) used TRIR results of concentrated TIPS-Pn solutions to show that pair–wise interactions *via* the TIPS side chain (Fig. 9g) activates optically dark symmetric stretching modes (*e.g.* the symmetric alkyne stretch at 2080 cm^{-1} and C–H stretching modes at higher wavenumbers). The activation was modelled by an additional ESA for the TRIR data in concentrated solutions. This finding was corroborated with concentration-dependent FTIR (Fig. 9e and f). Additionally, Fig. 9f shows similarity between the amorphous film and the concentrated solution, suggesting similar activation of dark vibrational modes is also expected in the amorphous film. One can rationalise this by the disordered arrangement of molecules in the amorphous films, which allows for the existence of pair–wise geometries where the TIPS groups interact. However, in the crystal stacking symmetry of TIPS-Pn, no such geometries are allowed and the activation of symmetry–forbidden interactions are not seen upon excitation (Fig. 9g).

Munson *et. al.* performed TRIR on amorphous TIPS-Pn films in a separate study, in which the ^{1}(TT) formation, separation and deactivation pathways were globally analysed.[98] However,

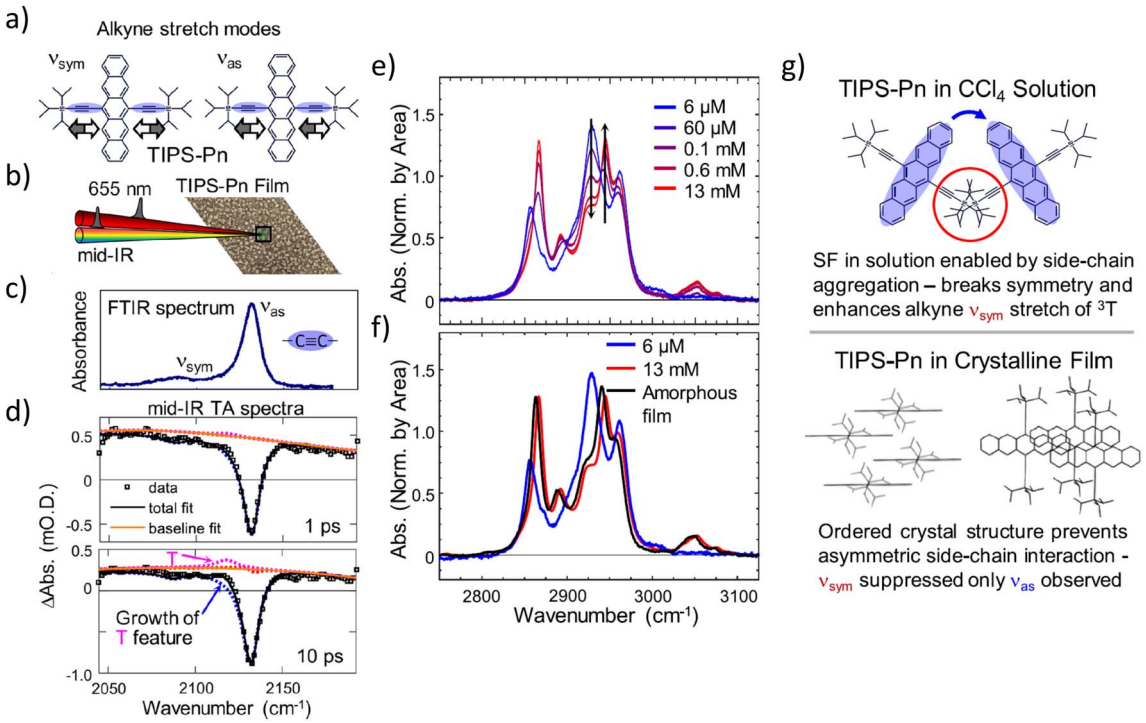

Fig. 9 SF of TIPS-Pn in solution probed with vibrational spectroscopy. (a) The alkyne symmetric and anti-symmetric stretches. (b) Schematic of the TRIR experiment (c) the FTIR spectra of TIPS-Pn solutions and (d) the TRIR spectra at 1 ps and 10 ps showing the growth in the triplet feature at 2120 cm^{-1}. (e) The concentation dependent FTIR spectrum in the C–H stretch region (f) solution state and the amorphous film FTIR in the C–H stretch region (g) Illustration of SB upon molecular interaction in solution and the solid state crystal structure symmetry of TIPS-Pn. Figure reprinted with permission from source.[51] Copyright AIP Publishing, 2019.

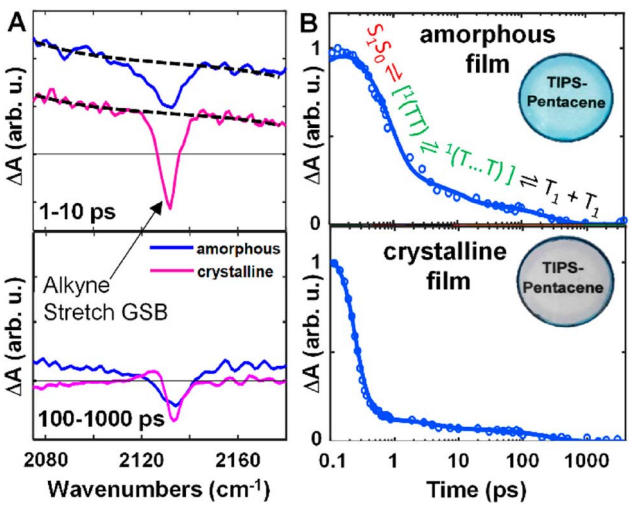

Fig. 10 TRIR study of crystalline and amorphous films of TIPS-Pn (A) the TRIR spectra in the first 10 ps focusing on the alkyne stretch region. (B) The SF kinetics based on the broad absorption assigned to the S_1 or a multi-electron state. Figure reprinted with permission from source.[98] Copyright American Chemical Society, 2020.

the activation of symmetry forbidden modes was not directly modelled in the kinetic analysis for the amorphous film. From the background-corrected data in (Fig. 10A), GSB features in the amorphous sample were broadened compared to those of the crystalline sample and there was a rising positive feature towards lower wavenumbers. It is worth further comparing the transient vibrational spectral signatures of these crystalline or amorphous thin films in lower and higher wavenumber regions and establish the correlation between the kinetics of SB modes and the formation of different transient species such as the ^{1}(TT) and the ^{1}(T···T) states.

TRIR studies have also been useful for providing vibrational fingerprints of SF intermediates in crystalline hexacene films.[126] In this system, the authors also observed rare vibrational stimulated emission at 1620 cm^{-1} (this mode does not correspond to any ground state IR absorption). The TRIR technique offers several advantages for solid-state material characterisation: (1) no solvent is present that can interfere with the quality of the TRIR signal; (2) optically opaque or scattering materials, *e.g.* thick films can be characterised since mid-IR radiation is still transmittable;[127] (3) vibrational transitions have smaller bandwidth and (4) the vibrational frequencies can be readily obtained by computational chemistry if the structure of the system is known. However, electron–phonon coupling usually yields a polaron signal as a broad background in TRIR measurements and should be carefully fitted and removed to extract distinct vibrational peaks. In addition, low oscillator strengths of vibrational transitions compared to electronic transitions generally require higher laser fluence to be used in TRIR measurements compared to TAS experiments. Fluence-dependent studies should be carefully conducted before comparing results acquired by different methods as SF

dynamics is usually highly dependent on excitation fluence.[128,129] Additionally, pump laser-induced annealing is sometimes observed at higher fluences,[98] especially for amorphous films, posing difficulties in data acquisition and analysis.

Time-resolved Raman techniques (*e.g.* fs stimulated Raman spectroscopy (fsSRS)) are also powerful tools in probing vibrational information during SF processes.[99,130–133] Several studies by the Frontiera group established the vibrational markers that indicate the formation of ^{1}(TT) and its subsequent separation in single-crystal rubrene (orthorhombic). Bera *et. al.*,[132] in their first study, identified the ESA at 1660 cm^{-1} with a rise time constant of 240 fs, which was assigned to the ^{1}(TT) state, and the fsSRS signals at 1430 cm^{-1} and 1542 cm^{-1} shift to higher wavenumbers and this reflects a structural rearrangement during triplet separation. Informed by this study, the authors later designed substituted rubrene and monitored the SF and triplet separation and the electronic density in the tetracene backbone using a combination of fsSRS and density functional theory.[99] The authors also provided guidelines on designing and optimising materials and assessing the SF performance with a combination of optical, vibrational spectroscopy and computational methods.[99,131] Hart *et. al.* performed fsSRS studies on pentacene single crystals, and observed the splitting and shifting of the ring vibrational modes around 1360 cm^{-1}.[59] The computational frequencies of the radical cation and anion were in agreement with the frequency shifts, directly hinting to a CT-type intermediate. In this case, the formation of a CT state will induce SB, therefore, identifying SB-activated vibrational modes using a combination of TRIR and fsSRS could be extremely useful in consolidating the assignment of the CT intermediate.

4.4 Multidimensional spectroscopy

2D electronic spectroscopy (2DES) has also attracted growing interest and demonstrated the ability to study vibronically coherent SF mechanisms.[45,56,100,134–136] Reviews on the principle and other applications of this technique can be found in literature.[137] The challenging experimental aspects have resulted in very few applications of this technique in solid-state SF studies. Wang *et. al.*[56] used polarisation-dependent 2DES to analyse coherent vibrations in tetracene single crystals, and it was found that the coupling to higher-energy vibrational modes lowers the energy gap between the singlet and triplet pair states. The authors used collinear pump pulse replicated with a Mach–Zehnder interferometer, and the phase stabilised with active feedback electronics, allowing for independent tuning of the pump–probe polarisations. When the polarisation of the probe is perpendicular to that of the pump, an additional ESA feature at 2.28 eV (not observed with parallel probe), and broad features centred at 1.54 eV were observed and attributed to the T_1 and ^{1}(TT) states. The onset of signal at 1.54 eV is independent of excitation energies and arises prior to thermal relaxation, hinting towards the coherent formation of lower excitonic and ^{1}(TT) states. Oscillations in GSB dynamics revealed two low frequency modes (131 cm^{-1} and 313 cm^{-1}) related to the $S_1 \leftarrow S_0$ transition. The higher frequency modes at 617 cm^{-1} and 750 cm^{-1} are signatures of the $S_1^* \leftarrow S_0$ excitation. The beating amplitudes are polarisation-dependent for the modes at 313 cm^{-1} and 750 cm^{-1}, and a distinct beating resonance near 2.42 eV is markedly different from that originated from the S_1 resonance. This newly observed beating behaviour was explained by the mixing of the ^{1}(TT) state with a hot S_1 state of the J-aggregates in the crystal through vibronic interactions. Yoshida *et. al.* performed temperature-dependent 2DES characterisation on ultra-thin tetracene films in reflectance geometry.[138] The authors examined the spectral diffusion of the lowest excitation with 30 fs temporal resolution. The frequency correlation function (FFCF) contained two components with 400 and 80 fs time constants. The former is attributed to the coupling to the phonon bath, and the latter component has temperature-dependent magnitude, assigned to the coupling between a low-frequency phonon mode and a high-frequency intramolecular vibrational mode. Although this study does not address the SF directly, the same interaction mechanisms could aid the analysis of the mechanism of ultrafast SF in tetracene thin films.

Whilst 2DES and its variations have been applied to study SF, many other 2D techniques have not been explored in the field yet. Oliver *et. al.* summarised recent advances of multidimensional spectroscopy.[139] To gain further insight into the role of SB vibrations in the activation of SF, spectroscopic methods involving targeted vibrational pre-excitation can be informative. A pulse sequence of mid-IR (narrow band), followed by a regular TAS pulse sequence after short delay time (before vibrational relaxation) can be readily achieved with an additional mid-IR difference frequency generator. Vibrationally promoted electronic resonance (VIPER) spectroscopy[140,141] is a relatively newly-emerged multi-dimensional IR spectroscopic technique with vibrational pre-excitation. This technique has been applied to controlling isotope-selective photochemistry,[142] and is yet to be explored in the context of SF. Another technique, 2D electronic-vibrational spectroscopy (2DEVS)[143–145] has been developed in the past decade and applied to photosynthetic systems[146] and molecular complexes.[147] This technique has the potential to offer great insights into the interaction between molecular vibrations and electronic transitions on a ps timescale for SF systems.

5 Conclusions and future directions

To summarise, this perspective provides a brief review of recent work relevant to solid-state SF materials. Due to the potential inhomogeneity and variation in morphology of solid-state materials in the application to photovoltaic devices, the effects of local symmetry, packing arrangement, and electronic environments must be studied independently before moving to a more complex system. Model systems, including dimers and oligomers, nanoparticles, and aggregates can aid to understand pair–wise interactions and the morphological effects on triplet generation and decay. The interpretations can be generalised to understand solid-state systems with careful considerations. Strategies for altering molecular stacking *via* substituents and crystallisation conditions have been explored to produce larger

solid structures with well-defined morphology. Self-assembly as a method of controlling packing arrangement has been explored in the past[148,149] but more in-depth spectroscopic characterisation in such systems remains an open area of research. The studies of SF in nanoparticles and aggregates are mostly conducted in solution and the data collected represent an ensemble of particles. Combining time-resolved micro-spectroscopy with optical trapping[150] can further enhance our understanding of the correlation between local environments and SF mechanisms. The understanding gained from this will aid decision making in molecular designs. In systems where local SB promotes SF pathways, side-chain substitutions that favour the formation of crystalline domains of various orientations would be beneficial for SF efficiencies. Conversely, molecular engineering to ensure uniform crystal structure formation is desired.

In addition, we have discussed recent progress in spectroscopic investigations of solid-state SF materials and highlighted the importance of microscopy and vibrational spectroscopy to understand the effects of local morphological disorder on the SF mechanisms, and to date, many conventional SF materials have still been debated regarding their SF mechanisms. Systematic studies employing time-resolved spectroscopic techniques to probe key electronic and vibrational signatures of intermediates, together with necessary magnetic-field and temperature-dependent measurements, are necessary for more conclusive assignments of SF pathways. Here, we outline an integrated protocol for studying novel and existing SF systems with mechanistic complexity. (1) In dilute solutions of monomers, ultrafast TAS in the vis-NIR or TRIR in the MIR region can establish spectral signatures of S_1 and potentially T_1 (if ISC is a pathway). (2) In concentrated solutions where SF occurs, spectral signatures of intermediate species including the ^{1}(TT) state can be extracted *via* rigorous kinetic modelling and global targeted analysis. If entangled states cannot be separated in all spectral regions, we can separate states with different spin multiplicities with the aid of magnetic field dependent TAS and/or trEPR for spin dynamics evolving on longer timescales. (3) For solid state systems, all the above-mentioned characterisation methods are powerful in understanding the average behaviour of the system. Films with inhomogeneity should be studied carefully with diffraction-limited microscopic methods and time-resolved microscopy to reveal effects of local morphological disorder on the SF kinetics. (4) Multidimensional optical and vibrational spectroscopies are powerful tools in identifying SB vibrations that facilitate coherent SF pathways.

Author contributions

Xinyue Xu prepared the manuscript, Prof. Trevor Smith and Dr Christopher R. Hall edited and reviewed the manuscript.

Conflicts of interest

There are no conflicts to declare.

Data availability

No primary research results, software or code have been included and no new data were generated or analysed as part of this review.

Acknowledgements

C. R. H. thanks the Australian Research Council for financial support (FT210100113).

Notes and references

1 S. Singh, W. Jones, W. Siebrand, B. Stoicheff and W. Schneider, *J. Chem. Phys.*, 1965, **42**, 330–342.
2 M. J. Tayebjee, K. N. Schwarz, R. W. MacQueen, M. Dvorak, A. W. Lam, K. P. Ghiggino, D. R. McCamey, T. W. Schmidt and G. J. Conibeer, *J. Phys. Chem. C*, 2016, **120**, 157–165.
3 M. A. Baldo, N. J. Ekins-Daukes, J. Y. Jiang, P. M. Pearce, T. W. Schmidt and M. J. Tayebjee, *ACS Energy Lett.*, 2025, **10**, 4830–4833.
4 R. J. Hudson, T. S. MacDonald, J. H. Cole, T. W. Schmidt, T. A. Smith and D. R. McCamey, *Nat. Rev. Chem.*, 2024, **8**, 136–151.
5 B. Daiber, K. van den Hoven, M. H. Futscher and B. Ehrler, *ACS Energy Lett.*, 2021, **6**, 2800–2808.
6 J. Xia, S. N. Sanders, W. Cheng, J. Z. Low, J. Liu, L. M. Campos and T. Sun, *Adv. Mater.*, 2017, **29**, 1601652.
7 J. Lee, P. Jadhav, P. D. Reusswig, S. R. Yost, N. J. Thompson, D. N. Congreve, E. Hontz, T. Van Voorhis and M. A. Baldo, *Acc. Chem. Res.*, 2013, **46**, 1300–1311.
8 A. J. Baldacchino, M. I. Collins, M. P. Nielsen, T. W. Schmidt, D. R. McCamey and M. J. Tayebjee, *Chem. Phys. Rev.*, 2022, **3**, 021304.
9 D. Casanova, *Chem. Rev.*, 2018, **118**, 7164–7207.
10 H. Kim and P. M. Zimmerman, *Phys. Chem. Chem. Phys.*, 2018, **20**, 30083–30094.
11 R. P. Steer, *J. Photochem. Photobiol., C*, 2019, **40**, 68–80.
12 N. Monahan and X.-Y. Zhu, *Annu. Rev. Phys. Chem.*, 2015, **66**, 601–618.
13 J. Li, H. Cao, Z. Zhang, S. Liu and Y. Xia, *Photonics*, 2022, 689.
14 P. M. Zimmerman, C. B. Musgrave and M. Head-Gordon, *Acc. Chem. Res.*, 2013, **46**, 1339–1347.
15 S. N. Sanders, A. B. Pun, K. R. Parenti, E. Kumarasamy, L. M. Yablon, M. Y. Sfeir and L. M. Campos, *Chem*, 2019, **5**, 1988–2005.
16 M. B. Smith and J. Michl, *Chem. Rev.*, 2010, **110**, 6891–6936.
17 M. B. Smith and J. Michl, *Annu. Rev. Phys. Chem.*, 2013, **64**, 361–386.
18 W.-L. Chan, T. C. Berkelbach, M. R. Provorse, N. R. Monahan, J. R. Tritsch, M. S. Hybertsen, D. R. Reichman, J. Gao and X.-Y. Zhu, *Acc. Chem. Res.*, 2013, **46**, 1321–1329.
19 A. Japahuge and T. Zeng, *ChemPlusChem*, 2018, **83**, 146–182.
20 W. Kim and A. J. Musser, *Adv. Phys.:X*, 2021, **6**, 1918022.

21 K. Miyata, F. S. Conrad-Burton, F. L. Geyer and X.-Y. Zhu, *Chem. Rev.*, 2019, **119**, 4261–4292.
22 R. M. Young and M. R. Wasielewski, *Acc. Chem. Res.*, 2020, **53**, 1957–1968.
23 T. Ullrich, D. Munz and D. M. Guldi, *Chem. Soc. Rev.*, 2021, **50**, 3485–3518.
24 R. Casillas, I. Papadopoulos, T. Ullrich, D. Thiel, A. Kunzmann and D. M. Guldi, *Energy Environ. Sci.*, 2020, **13**, 2741–2804.
25 T. Wang, H. Liu, X. Wang, L. Tang, J. Zhou, X. Song, L. Lv, W. Chen, Y. Chen and X. Li, *J. Mater. Chem. A*, 2023, **11**, 8515–8539.
26 K. Wang, X. Chen, J. Xu, S. Peng, D. Wu and J. Xia, *Macromol. Rapid Commun.*, 2024, **45**, 2300241.
27 Z. Wang, X. Xie and H. Ma, *Wiley Interdiscip. Rev.: Comput. Mol. Sci.*, 2025, **15**, 70002.
28 S. L. Bayliss, L. R. Weiss, A. Rao, R. H. Friend, A. D. Chepelianskii and N. C. Greenham, *Phys. Rev. B*, 2016, **94**, 045204.
29 S. Ito, T. Nagami and M. Nakano, *J. Photochem. Photobiol., C*, 2018, **34**, 85–120.
30 S. Lukman, K. Chen, J. M. Hodgkiss, D. H. Turban, N. D. Hine, S. Dong, J. Wu, N. C. Greenham and A. J. Musser, *Nat. Commun.*, 2016, **7**, 13622.
31 E. A. Margulies, N. Kerisit, P. Gawel, C. M. Mauck, L. Ma, C. E. Miller, R. M. Young, N. Trapp, Y.-L. Wu, F. Diederich, *et al.*, *J. Phys. Chem. C*, 2017, **121**, 21262–21271.
32 A. M. Alvertis, S. Lukman, T. J. Hele, E. G. Fuemmeler, J. Feng, J. Wu, N. C. Greenham, A. W. Chin and A. J. Musser, *J. Am. Chem. Soc.*, 2019, **141**, 17558–17570.
33 R. S. Mattos, I. Burghardt, A. J. Aquino, T. M. Cardozo and H. Lischka, *J. Am. Chem. Soc.*, 2022, **144**, 23492–23504.
34 L. Xue, H. Huang, S. Wu, X. Song, G. Lu, S. Cheng and Y. Bu, *J. Chem. Theory Comput.*, 2023, **19**, 3806–3816.
35 X. Zhao, J. P. O'Connor, J. D. Schultz, Y. J. Bae, C. Lin, R. M. Young and M. R. Wasielewski, *J. Phys. Chem. B*, 2021, **125**, 6945–6954.
36 K. Sun, Q. Xu, L. Chen, M. F. Gelin and Y. Zhao, *J. Chem. Phys.*, 2020, **153**, 194106.
37 E. A. Margulies, C. E. Miller, Y. Wu, L. Ma, G. C. Schatz, R. M. Young and M. R. Wasielewski, *Nat. Chem.*, 2016, **8**, 1120–1125.
38 L. Ahrens, N. Wollscheid, J. Han, O. Kefer, F. Rominger, A. Roozbeh, J. Freudenberg, A. Dreuw, U. H. Bunz and T. Buckup, *J. Phys. Chem. B*, 2021, **125**, 13235–13245.
39 Y. Hong, M. Rudolf, M. Kim, J. Kim, T. Schembri, A.-M. Krause, K. Shoyama, D. Bialas, M. I. Röhr, T. Joo, *et al.*, *Nat. Commun.*, 2022, **13**, 4488.
40 R. J. Hudson, A. N. Stuart, J. M. de la Perrelle, D. M. Huang and T. W. Kee, *J. Phys. Chem. C*, 2021, **125**, 21559–21570.
41 R. P. Steer, *Phys. Chem. Chem. Phys.*, 2023, **25**, 23384–23394.
42 A. N. Stuart, P. C. Tapping, E. Schrefl, D. M. Huang and T. W. Kee, *J. Phys. Chem. C*, 2019, **123**, 5813–5825.
43 R. D. Pensack, C. Grieco, G. E. Purdum, S. M. Mazza, A. J. Tilley, E. E. Ostroumov, D. S. Seferos, Y.-L. Loo, J. B. Asbury, J. E. Anthony, *et al.*, *Mater. Horiz.*, 2017, **4**, 915–923.
44 M. Chen, Y. J. Bae, C. M. Mauck, A. Mandal, R. M. Young and M. R. Wasielewski, *J. Am. Chem. Soc.*, 2018, **140**, 9184–9192.
45 A. Mandal, M. Chen, E. D. Foszcz, J. D. Schultz, N. M. Kearns, R. M. Young, M. T. Zanni and M. R. Wasielewski, *J. Am. Chem. Soc.*, 2018, **140**, 17907–17914.
46 Y. Zhou, W. Ni, L. Ma, L. Sun, J. Zhao and G. G. Gurzadyan, *J. Phys. Chem. C*, 2022, **126**, 17212–17222.
47 L. Xue, X. Song, Y. Feng, S. Cheng, G. Lu and Y. Bu, *J. Am. Chem. Soc.*, 2020, **142**, 17469–17479.
48 H. Tamura, M. Huix-Rotllant, I. Burghardt, Y. Olivier and D. Beljonne, *Phys. Rev. Lett.*, 2015, **115**, 107401.
49 D. R. Maslennikov, M. Maimaris, H. Ning, X. Zheng, N. Mondal, V. V. Bruevich, S. M. Pratik, Y. Dong, J. W. Tisch, A. J. Musser, *et al.*, *J. Am. Chem. Soc.*, 2025, **147**, 23536–23544.
50 L.-C. Lin, R. D. Dill, K. J. Thorley, S. R. Parkin, J. E. Anthony, J. C. Johnson and N. H. Damrauer, *J. Phys. Chem.*, 2024, **128**, 3982–3992.
51 C. Grieco, G. S. Doucette, K. T. Munson, J. R. Swartzfager, J. M. Munro, J. E. Anthony, I. Dabo and J. B. Asbury, *J. Chem. Phys.*, 2019, **151**, 154701.
52 N. Maity, W. Kim, N. A. Panjwani, A. Kundu, K. Majumder, P. Kasetty, D. Mishra, R. Bittl, J. Nagesh, J. Dasgupta, *et al.*, *Nat. Commun.*, 2022, **13**, 5244.
53 R. D. Pensack, E. E. Ostroumov, A. J. Tilley, S. Mazza, C. Grieco, K. J. Thorley, J. B. Asbury, D. S. Seferos, J. E. Anthony and G. D. Scholes, *J. Phys. Chem. Lett.*, 2016, **7**, 2370–2375.
54 C. Grieco, E. R. Kennehan, H. Kim, R. D. Pensack, A. N. Brigeman, A. Rimshaw, M. M. Payne, J. E. Anthony, N. C. Giebink, G. D. Scholes, *et al.*, *J. Phys. Chem. C*, 2018, **122**, 2012–2022.
55 A. J. Musser, M. Liebel, C. Schnedermann, T. Wende, T. B. Kehoe, A. Rao and P. Kukura, *Nat. Phys.*, 2015, **11**, 352–357.
56 G. Wang, C. Zhang, Z. Liu, R. Wang, H. Ma, X. Wang and M. Xiao, *J. Phys. Chem.*, 2020, **124**, 10447–10456.
57 D. G. Bossanyi, M. Matthiesen, R. Jayaprakash, S. Bhattacharya, J. Zaumseil and J. Clark, *Faraday Discuss.*, 2024, **250**, 162–180.
58 Y. Liu, X. Yang, L. Ye, H. Ma and H. Zhu, *Aggregate*, 2023, **4**, 347.
59 S. M. Hart, W. R. Silva and R. R. Frontiera, *Chem. Sci.*, 2018, **9**, 1242–1250.
60 L. M. Yablon, S. N. Sanders, K. Miyazaki, E. Kumarasamy, G. He, B. Choi, N. Ananth, M. Y. Sfeir and L. M. Campos, *Mater. Horiz.*, 2022, **9**, 462–470.
61 S. Nakamura, H. Sakai, H. Nagashima, M. Fuki, K. Onishi, R. Khan, Y. Kobori, N. V. Tkachenko and T. Hasobe, *J. Phys. Chem. C*, 2021, **125**, 18287–18296.
62 C. Hetzer, D. M. Guldi and R. R. Tykwinski, *Chem.–Eur. J.*, 2018, **24**, 8245–8257.

63 N. Alagna, J. L. P. Lustres, A. Roozbeh, J. Han, S. Hahn, F. J. Berger, J. Zaumseil, A. Dreuw, U. H. Bunz and T. Buckup, *J. Phys. Chem. B*, 2020, **124**, 9163–9174.
64 N. V. Korovina, J. Joy, X. Feng, C. Feltenberger, A. I. Krylov, S. E. Bradforth and M. E. Thompson, *J. Am. Chem. Soc.*, 2018, **140**, 10179–10190.
65 W. Kim, N. A. Panjwani, K. Krishnapriya, K. Majumder, J. Dasgupta, R. Bittl, S. Patil and A. J. Musser, *Cell Rep. Phys. Sci.*, 2024, **5**, 102045.
66 A. Aster, F. Zinna, C. Rumble, J. Lacour and E. Vauthey, *J. Am. Chem. Soc.*, 2021, **143**, 2361–2371.
67 K. Majumder, S. Mukherjee, N. A. Panjwani, J. Lee, R. Bittl, W. Kim, S. Patil and A. J. Musser, *J. Am. Chem. Soc.*, 2023, **145**, 20883–20896.
68 I. Papadopoulos, Y. Gao, C. Hetzer, R. R. Tykwinski and D. M. Guldi, *ChemPhotoChem*, 2020, **4**, 5168–5174.
69 N. H. Damrauer and J. L. Snyder, *J. Phys. Chem. Lett.*, 2015, **6**, 4456–4462.
70 A. Aster, G. Licari, F. Zinna, E. Brun, T. Kumpulainen, E. Tajkhorshid, J. Lacour and E. Vauthey, *Chem. Sci.*, 2019, **10**, 10629–10639.
71 L. Lv, H. Liu, T. Li, B. Cui, T. Wang, X. Song, W. Chen, Y. Chen and X. Li, *J. Mater. Chem. C*, 2023, **11**, 16782–16791.
72 L. Estergreen, A. R. Mencke, D. E. Cotton, N. V. Korovina, J. Michl, S. T. Roberts, M. E. Thompson and S. E. Bradforth, *Acc. Chem. Res.*, 2022, **55**, 1561–1572.
73 B. Kang and W. Kim, *ChemPhotoChem*, 2024, **8**, e202300237.
74 Y. Wu, J. Zhou, B. T. Phelan, C. M. Mauck, J. F. Stoddart, R. M. Young and M. R. Wasielewski, *J. Am. Chem. Soc.*, 2017, **139**, 14265–14276.
75 C. Lin, T. Kim, J. D. Schultz, R. M. Young and M. R. Wasielewski, *Nat. Chem.*, 2022, **14**, 786–793.
76 G. He, E. Busby, K. Appavoo, Q. Wu, J. Xia, L. M. Campos and M. Y. Sfeir, *J. Chem. Phys.*, 2020, **153**, 244902.
77 C. M. Mauck, P. E. Hartnett, Y.-L. Wu, C. E. Miller, T. J. Marks and M. R. Wasielewski, *Chem. Mater.*, 2017, **29**, 6810–6817.
78 J. Zhou, H. Liu, S. Liu, P. Su, W. Wang, Z. Li, Z. Liu, Y. Chen, Y. Dong and X. Li, *J. Phys. Chem. B*, 2022, **126**, 6483–6492.
79 Z. Tang, S. Zhou, H. Liu, X. Wang, S. Liu, L. Shen, X. Lu and X. Li, *Mater. Chem. Front.*, 2020, **4**, 2113–2125.
80 J. N. Mastron, S. T. Roberts, R. E. McAnally, M. E. Thompson and S. E. Bradforth, *J. Phys. Chem. B*, 2013, **117**, 15519–15526.
81 R. D. Pensack, A. J. Tilley, S. R. Parkin, T. S. Lee, M. M. Payne, D. Gao, A. A. Jahnke, D. G. Oblinsky, P.-F. Li, J. E. Anthony, *et al.*, *J. Am. Chem. Soc.*, 2015, **137**, 6790–6803.
82 G. Huang, J. Li, Z. Zhou, Z. Huang, W. Kong, F. Zhang, Y. Zeng, G. Liu, T. He and L. Ma, *Ultrafast Sci.*, 2024, **4**, 0057.
83 L. Wang, W. Cai, J. Sun, Y. Wu, B. Zhang, X. Tian, S. Guo, W. Liang, H. Fu and J. Yao, *J. Phys. Chem. Lett.*, 2021, **12**, 12276–12282.
84 B. Zhang, Y. Zhao and W. Liang, *J. Phys. Chem. C*, 2021, **125**, 1654–1664.
85 L. A. Martínez-Martínez, M. Du, R. F. Ribeiro, S. Kéna-Cohen and J. Yuen-Zhou, *J. Phys. Chem. Lett.*, 2018, **9**, 1951–1957.
86 G. Mayonado, K. T. Vogt, J. D. Van Schenck, L. Zhu, G. Fregoso, J. Anthony, O. Ostroverkhova and M. W. Graham, *J. Phys. Chem. C*, 2022, **126**, 4433–4445.
87 Y. Wu, K. Liu, H. Liu, Y. Zhang, H. Zhang, J. Yao and H. Fu, *J. Phys. Chem. Lett.*, 2014, **5**, 3451–3455.
88 Y. J. Bae, J. A. Christensen, G. Kang, J. Zhou, R. M. Young, Y.-L. Wu, R. P. Van Duyne, G. C. Schatz and M. R. Wasielewski, *J. Chem. Phys.*, 2019, **151**, 044501.
89 L. Shen, Z. Tang, X. Wang, H. Liu, Y. Chen and X. Li, *Phys. Chem. Chem. Phys.*, 2018, **20**, 22997–23006.
90 C. Grieco, G. S. Doucette, R. D. Pensack, M. M. Payne, A. Rimshaw, G. D. Scholes, J. E. Anthony and J. B. Asbury, *J. Am. Chem. Soc.*, 2016, **138**, 16069–16080.
91 C. Grieco, G. S. Doucette, J. M. Munro, E. R. Kennehan, Y. Lee, A. Rimshaw, M. M. Payne, N. Wonderling, J. E. Anthony, I. Dabo, *et al.*, *Adv. Funct. Mater.*, 2017, **27**, 1703929.
92 Z. T. Armstrong, M. B. Kunz, A. C. Jones and M. T. Zanni, *J. Phys. Chem. C*, 2020, **124**, 15123–15131.
93 D. M. de Clercq, M. I. Collins, N. P. Sloane, J. Feng, D. R. McCamey, M. J. Tayebjee, M. P. Nielsen and T. W. Schmidt, *Chem. Sci.*, 2024, **15**, 6402–6409.
94 R. t. Vulchi, V. Morgunov, R. Junjuri and T. Bocklitz, *Molecules*, 2024, **29**, 4748.
95 D. G. Bossanyi, M. Matthiesen, S. Wang, J. A. Smith, R. C. Kilbride, J. D. Shipp, D. Chekulaev, E. Holland, J. E. Anthony, J. Zaumseil, *et al.*, *Nat. Chem.*, 2021, **13**, 163–171.
96 K. Wang, H. Huang, K. Xu, S. Peng, X. You, X. Chen, J. Xu, D. Wu and J. Xia, *J. Phys. Chem. Lett.*, 2023, **14**, 4822–4829.
97 I. H. Van Stokkum, D. S. Larsen and R. Van Grondelle, *Biochim. Biophys. Acta Bioenerg.*, 2004, **1657**, 82–104.
98 K. T. Munson, J. Gan, C. Grieco, G. S. Doucette, J. E. Anthony and J. B. Asbury, *J. Phys. Chem. C*, 2020, **124**, 23567–23578.
99 K. Bera, S. Y. Kwang and R. R. Frontiera, *J. Phys. Chem. C*, 2020, **124**, 25163–25174.
100 A. A. Bakulin, S. E. Morgan, T. B. Kehoe, M. W. Wilson, A. W. Chin, D. Zigmantas, D. Egorova and A. Rao, *Nat. Chem.*, 2016, **8**, 16–23.
101 T. S. Volek, Z. T. Armstrong, J. K. Sowa, K. S. Wilson, M. Bohlmann Kunz, K. Bera, M. Koble, R. R. Frontiera, P. J. Rossky, M. T. Zanni, *et al.*, *J. Phys. Chem. Lett.*, 2023, **14**, 11497–11505.
102 A. M. Berghuis, T. Raziman, A. Halpin, S. Wang, A. G. Curto and J. G. Rivas, *J. Phys. Chem. Lett.*, 2021, **12**, 1360–1366.
103 A. C. Jones, N. M. Kearns, J.-J. Ho, J. T. Flach and M. T. Zanni, *Nat. Chem.*, 2020, **12**, 40–47.
104 P. J. Brown, M. L. Williams, S. Nakamura, J. R. Palmer, R. M. Young and M. R. Wasielewski, *J. Phys. Chem. C*, 2024, **128**, 58–66.
105 M. L. Williams, I. Schlesinger, C. E. Ramirez, R. M. Jacobberger, P. J. Brown, R. M. Young and M. R. Wasielewski, *J. Phys. Chem. C*, 2022, **126**, 10287–10297.
106 E. M. Bu Ali, A. Bertran, G. Moise, S. Wang, R. C. Kilbride, J. E. Anthony, C. E. Tait and J. Clark, *J. Am. Chem. Soc.*, 2025, **147**, 28638–28650.

107 S. Weber, *EPR Spectroscopy: Fundamentals and Methods*, 2018, vol. 195, pp. 195–626.
108 S. Richert, C. E. Tait and C. R. Timmel, *J. Magn. Reson.*, 2017, **280**, 103–116.
109 D. Lubert-Perquel, E. Salvadori, M. Dyson, P. N. Stavrinou, R. Montis, H. Nagashima, Y. Kobori, S. Heutz and C. W. Kay, *Nat. Commun.*, 2018, **9**, 4222.
110 T. Quintes, S. Weber and S. Richert, *J. Phys. Chem.*, 2025, **129**, 3375–3388.
111 M. J. Tayebjee, S. N. Sanders, E. Kumarasamy, L. M. Campos, M. Y. Sfeir and D. R. McCamey, *Nat. Phys.*, 2017, **13**, 182–188.
112 J. K. Bindra, D. Malinowski, B. Salcido-Santacruz, G. He, M. Y. Sfeir, L. M. Campos, J. Niklas and O. G. Poluektov, *J. Am. Chem. Soc.*, 2025, **147**, 25672–25681.
113 R. D. Dill, K. E. Smyser, B. K. Rugg, N. H. Damrauer and J. D. Eaves, *Nat. Commun.*, 2023, **14**, 1180.
114 N. A. Pace, B. K. Rugg, C. H. Chang, O. G. Reid, K. J. Thorley, S. Parkin, J. E. Anthony and J. C. Johnson, *Chem. Sci.*, 2020, **11**, 7226–7238.
115 S. L. Bayliss, L. Weiss, F. Kraffert, D. Granger, J. Anthony, J. Behrends and R. Bittl, *Phys. Rev. X*, 2020, **10**, 021070.
116 T. S. MacDonald, M. J. Tayebjee, M. I. Collins, E. Kumarasamy, S. N. Sanders, M. Y. Sfeir, L. M. Campos and D. R. McCamey, *J. Am. Chem. Soc.*, 2023, **145**, 15275–15283.
117 G. He, K. R. Parenti, P. J. Budden, J. Niklas, T. Macdonald, E. Kumarasamy, X. Chen, X. Yin, D. R. McCamey, O. G. Poluektov, *et al.*, *J. Am. Chem. Soc.*, 2023, **145**, 22058–22068.
118 J. Hausch, A. J. Berges, C. Zeiser, T. Rammler, A. Morlok, J. Bredehoft, S. Hammer, J. Pflaum, C. J. Bardeen and K. Broch, *J. Phys. Chem. C*, 2022, **126**, 6686–6693.
119 J. Hausch, N. Hofeditz, J. Bredehoft, S. Hammer, J. Pflaum, K. Broch, M. Gerhard and F. Schreiber, *J. Phys. Chem. C*, 2023, **127**, 3778–3786.
120 P. Petelenz and M. Snamina, *J. Phys. Chem. Lett.*, 2016, **7**, 1913–1916.
121 B. Dereka, A. Rosspeintner, Z. Li, R. Liska and E. Vauthey, *J. Am. Chem. Soc.*, 2016, **138**, 4643–4649.
122 B. Dereka, A. Rosspeintner, R. Stezycki, C. Ruckebusch, D. T. Gryko and E. Vauthey, *J. Phys. Chem. Lett.*, 2017, **8**, 6029–6034.
123 B. Dereka, E. Balanikas, A. Rosspeintner, Z. Li, R. Liska and E. Vauthey, *J. Phys. Chem. Lett.*, 2024, **15**, 8280–8286.
124 E. Vauthey, *J. Phys. Chem. Lett.*, 2022, **13**, 2064–2071.
125 K. T. Munson, E. R. Kennehan and J. B. Asbury, *J. Mater. Chem. C*, 2019, **7**, 5889–5909.
126 G.-H. Deng, Q. Wei, J. Han, Y. Qian, J. Luo, A. R. Harutyunyan, G. Chen, H. Bian, H. Chen and Y. Rao, *J. Chem. Phys.*, 2019, **151**, 054703.
127 K. Zhang, X. Xu, J. Qiao, Y. Xu, W. Zhang, M. Zhou, Y. Wang, T. He, H. Yin, X. Du, *et al.*, *Nano Energy*, 2025, **134**, 110546.
128 Y. Ishibashi, Y. Inoue and T. Asahi, *Photochem. Photobiol. Sci.*, 2016, **15**, 1304–1309.
129 J. J. Burdett, D. Gosztola and C. J. Bardeen, *J. Chem. Phys.*, 2011, **135**, 214508.
130 B. Peng, Z. Wang, J. Jiang, Y. Huang and W. Liu, *J. Chem. Phys.*, 2024, **160**, 194304.
131 K. Bera, C. J. Douglas and R. R. Frontiera, *Chem. Sci.*, 2021, **12**, 13825–13835.
132 K. Bera, C. J. Douglas and R. R. Frontiera, *J. Phys. Chem. Lett.*, 2017, **8**, 5929–5934.
133 S. R. Ellis, D. R. Dietze, T. Rangel, F. Brown-Altvater, J. B. Neaton and R. A. Mathies, *J. Phys. Chem.*, 2019, **123**, 3863–3875.
134 J. D. Schultz, J. Y. Shin, M. Chen, J. P. O'Connor, R. M. Young, M. A. Ratner and M. R. Wasielewski, *J. Am. Chem. Soc.*, 2021, **143**, 2049–2058.
135 O. Kefer, P. V. Kolesnichenko, L. Ahrens, J. Freudenberg, U. H. Bunz and T. Buckup, *arXiv*, 2024, preprint arXiv:2403.05163, DOI: 10.48550/arXiv.2403.05163.
136 T. Kim, C. Lin, J. D. Schultz, R. M. Young and M. R. Wasielewski, *J. Am. Chem. Soc.*, 2022, **144**, 11386–11396.
137 E. Fresch, F. V. Camargo, Q. Shen, C. C. Bellora, T. Pullerits, G. S. Engel, G. Cerullo and E. Collini, *Nat. Rev. Methods Primers*, 2023, **3**, 84.
138 T. Yoshida, K. Watanabe, M. Petrovic and M. Kralj, *J. Phys. Chem. Lett.*, 2020, **11**, 5248–5254.
139 T. A. Oliver, *R. Soc. Open Sci.*, 2018, **5**, 171425.
140 J. von Cosel, J. Cerezo, D. Kern-Michler, C. Neumann, L. J. van Wilderen, J. Bredenbeck, F. Santoro and I. Burghardt, *J. Chem. Phys.*, 2017, **147**, 164116.
141 M. Horz, H. Masood, H. Brunst, J. Cerezo, D. Picconi, H. Vormann, M. S. Niraghatam, L. J. van Wilderen, J. Bredenbeck, F. Santoro, *et al.*, *J. Chem. Phys.*, 2023, **158**, 064201.
142 D. Kern-Michler, C. Neumann, N. Mielke, L. J. van Wilderen, M. Reinfelds, J. von Cosel, F. Santoro, A. Heckel, I. Burghardt and J. Bredenbeck, *J. Am. Chem. Soc.*, 2018, **140**, 926–931.
143 N. H. C. Lewis, H. Dong, T. A. A. Oliver and G. R. Fleming, *J. Chem. Phys.*, 2015, **143**, 124203.
144 M. Cho and G. R. Fleming, *J. Phys. Chem. B*, 2020, **124**, 11222–11235.
145 J. D. Gaynor and M. Khalil, *J. Chem. Phys.*, 2017, **147**, 094202.
146 E. C. Wu, E. A. Arsenault, P. Bhattacharyya, N. H. Lewis and G. R. Fleming, *Faraday Discuss.*, 2019, **216**, 116–132.
147 P. Bhattacharyya and G. R. Fleming, *J. Phys. Chem. Lett.*, 2019, **10**, 2081–2089.
148 S. Masoomi-Godarzi, M. Liu, Y. Tachibana, L. Goerigk, K. P. Ghiggino, T. A. Smith and D. J. Jones, *Adv. Energy Mater.*, 2018, **8**, 1801720.
149 S. Masoomi-Godarzi, M. Liu, Y. Tachibana, V. D. Mitchell, L. Goerigk, K. P. Ghiggino, T. A. Smith and D. J. Jones, *Adv. Energy Mater.*, 2019, **9**, 1901069.
150 A. Lehmuskero, P. Johansson, H. Rubinsztein-Dunlop, L. Tong and M. Kall, *ACS Nano*, 2015, **9**, 3453–3469.